Modelling the flight dynamics of the hang glider

M. V. Cook and M. Spottiswoode
Dynamics, Simulation and Control Group
Department of Aerospace Sciences
School of Engineering
Cranfield University
Bedfordshire, UK

ABSTRACT

The development of the non-linear equations of motion for the hang glider from first principles is described, including the complex geometry of control by pilot 'weight shift'. By making appropriate assumptions the linearised small perturbation equations are derived for the purposes of stability and control analysis. The mathematical development shows that control is effected not by pilot weight shift, but by centre of gravity shift and that lateral-directional control by this means is weak, and is accompanied by significant instantaneous adverse response.

The development of a comprehensive semi-empirical mathematical model of the flexible wing aerodynamics is described. In particular, the modelling attempts to quantify camber and twist dependencies. The performance of the model is shown to compare satisfactorily with measured hang glider wing data obtained in earlier full scale experiments. The mathematical aerodynamic model is then used to estimate the hang glider stability and control derivatives over the speed envelope for substitution into the linearised equations of motion.

Solution of the equations of motion is illustrated and the flight dynamics of the typical hang glider are described. In particular, the dynamic stability properties are very similar to those of a conventional aeroplane, but the predicted lateral directional stability margins are significantly larger. The depth of mathematical modelling employed enables the differences to be explained satisfactorily. The unique control properties of the hang glider are described in some detail. Pitch and roll control of the hang glider is an aerodynamic phenomenon and results from the pilot adjusting his position relative to the wing in order to generate out of trim aerodynamic control moments about the centre of gravity. Maximum control moments are limited by hang glider geometry which is dependent on the length of the pilot's arm. The pilot does not generate control moments directly by shifting his weight relative to the wing. The modelling thus described would seem to give a plausible description of the flight dynamics of the hang glider.

NOMENCLATURE

a_1	lift curve slope due to incidence
a_{21}	lift curve slope due to camber for $\alpha_R \geq 0$
a_{22}	lift curve slope due to camber for $\alpha_R < 0$
a_3	lift curve slope due to action of luff lines
arp	wing aerodynamic reference point
b	wingspan
c	chord

Paper No. 2993. Manuscript received 8 July 2005, revised version received 12 September 2005, accepted 11 October 2005.

c' reference chord (geometric mean chord)
cg centre of gravity
c_r wing root chord
c_t wing tip chord
c_y local chord at a spanwise co-ordinate y
C_D drag coefficient
C_L lift coefficient
C_m pitching moment coefficient
D drag
g acceleration due to gravity
I_x roll moment of inertia
I_{xz} product of inertia about the x and z axes
I_y pitch moment of inertia
I_z yaw moment of inertia
$k_1 \ldots k_6$ empirical aerodynamic constants
$l_1 \ldots l_5$ geometric constants
l_2 hang strap length
L lift; rolling moment
m mass
M pitching moment
M_{o_w} zero lift pitching moment of wing
M_p pilot moment ratio
M_w pitching moment due to wing
N yawing moment
o axis origin
p roll rate perturbation
q pitch rate perturbation
r yaw rate perturbation
s Laplace operator
S wing reference area
t time
T mode time constant
u axial velocity perturbation
U total axial velocity
v lateral velocity perturbation
V total lateral velocity; perturbed airspeed
V_0 steady equilibrium velocity
w normal velocity perturbation
W total normal velocity
x longitudinal co-ordinate of axis system
x_L point at which lift due to the action of luff lines acts on reference chord
X axial force
y lateral co-ordinate of axis system; wing spanwise co-ordinate
Y lateral force
z normal co-ordinate of axis system
Z normal force
α angle of incidence
α_L section incidence at which luffing commences
α_{RL} root incidence at which luff lines become tight
α'_{RL} root incidence at which luff lines impose maximum trailing edge reflex
α_R wing root (keel) incidence
δ longitudinal control angle
δ_x axial position perturbation due to a control input
δ_y lateral position perturbation due to a control input
δ_z normal position perturbation due to a control input
ε_T wing tip twist
ε_y wing twist at spanwise co-ordinate y
Δ transfer function denominator
ϕ roll attitude perturbation
ϕ_e equilibrium roll attitude
γ flight path angle perturbation (positive nose up)
Γ dihedral angle
θ pitch attitude perturbation
ω undamped natural frequency
ξ lateral control angle
ψ yaw attitude perturbation
ζ damping ratio

Subscripts and superscripts

a aerodynamic
c due to camber
dr of the dutch roll mode
e equilibrium
f of the control frame
g due to gravity
lat lateral reference
$long$ longitudinal reference
L due to action of luff lines
p of the pilot
ph of the phugoid mode
r of the roll subsidence mode
s of the spiral mode
sp of the short period pitching mode
ss steady state
w of the wing
y spanwise co-ordinate y
a due to incidence
$*$ equivalent total aerodynamic derivative

Examples of aerodynamic derivative notation

X_{a_e} steady aerodynamic axial force
X_u dimensionless derivative of axial force due to axial velocity
$\mathring{X}_u$ dimensional derivative of axial force due to axial velocity
X_u^* equivalent dimensionless derivative of axial force due to axial velocity
$\mathring{X}_u^*$ equivalent dimensional derivative of axial force due to axial velocity

1.0 INTRODUCTION

The flight dynamics, stability and control of the hang glider has been a research interest at Cranfield where the principal objective has been to improve the understanding of those aspects of flying qualities which determine the safety boundaries of the hang glider and the physical principles on which they depend. Although numerous studies have been made at Cranfield, the fundamental contribution to the research was made by Kilkenny[1] and that work established the foundation on which all subsequent research has been based. The original research included an experimental programme to measure the aerodynamic properties of a number of full scale hang glider wings and a purpose built mobile test rig[2] was developed for the purpose. This early research was undertaken with the support of the British Hang Gliding Association (BHGA) and some of its members actively participated in the experimental work. An interim summary of this aerodynamic modelling research was made by Cook and Kilkenny[3]. Further, full scale wind tunnel tests of hang glider pilots made by Kilkenny[4] completed the data base. The aerodynamic model thus achieved from these early studies has provided an invaluable resource for all subsequent research including that described in this paper.

Follow on research focused on the application of the classical theory of the longitudinal static stability of the conventional aeroplane to the hang glider, since it relates simply, with acceptable accuracy, to observable stability and control characteristics. Initial studies of this topic were made by Blake[5] which culminated in a description of the theory of the longitudinal static stability of the hang glider by Cook[6]. In this research it was discovered that the classical theory of the longitudinal static stability adapts easily to the

hang glider and, provided that the appropriate assumptions are made, equally simple parallel conclusions may be drawn concerning its stability and control characteristics.

It is evident that the aerodynamics of the hang glider wing are very non-linear due to its inherent flexibility. Since the non-linearity has an influence on stability and control a study was undertaken by Powton[7] which led to a better understanding of aerodynamic non-linearity in terms of wing camber and twist variation. This study was also successful in quantifying the effect of non-linearity on aerodynamic pitching moment, an important parameter in hang glider stability and control analysis.

Recent research studies have concentrated on the dynamic stability and control of the hang glider. Preliminary studies were made by Rollins[8] in which the emphasis was on longitudinal stability and control. This was followed by a comprehensive and substantial modelling exercise by Spottiswoode[9] covering both longitudinal and lateral-directional dynamic modelling. This research provides the basis for the present paper although the mathematical development is, of necessity, presented in a very much abbreviated form.

2.0 HISTORICAL PERSPECTIVE

Foot launched piloted gliders are as old as the history of aviation, although the modern hang glider has its roots in the space age. In the early 1960s NASA conducted experimental investigations into the use of flexible parawings as a means for the recovery of returning space vehicles. This concept was abandoned by NASA, but the light-weight two lobed parawing was developed by Rogallo into a rudimentary piloted glider. Thereafter the 'Rogallo' glider evolved rapidly into the modern hang glider and the history of that development is well documented.

Since the sport of hang gliding is a 'low cost' means to enjoy flying, the development of the hang glider has been largely empirical with only modest dependence on aeronautical theory. This is especially true for matters concerned with the stability, control and flying qualities of the hang glider. Consequently, very little published material deals with this topic with a few notable exceptions. One of the most comprehensive research studies to deal with aerodynamic modelling, stability and control was conducted by Kroo[10] in the early 1980s, with NASA support. The research considered several approaches to aerodynamic and aeroelastic modelling, which led naturally to the estimation of aerodynamic derivatives and to the development of the equations of motion of the hang glider.

Kroo[10] developed the small perturbation equations of motion for both longitudinal and lateral-directional dynamics of the hang glider. These were also used as a basis for the estimation of larger amplitude dynamics. Interestingly, Kroo showed that lowering the centre of gravity, equivalent to increasing the pilot moment ratio as defined by Cook[6], increases static pitch stability at high angle-of-attack. Kroo also showed that apparent mass, unsteady aerodynamic effects and wing flexibility, especially twist, are all important contributors to the flight dynamics of the hang glider.

More recent research by de Matteis[11,12] developed a small perturbation model of the hang glider-pilot system, for both longitudinal and lateral-directional motion. Significantly, the aerodynamic modelling assumes a rigid wing, on the basis that the velocity dependence of the aerodynamic derivatives could be added at a later stage. It is acknowledged that the flexible wing aerodynamic 'shape' is very much velocity dependent and cannot be ignored except in the most preliminary model. The flight dynamics analysis describes the stability and control characteristics of the hang glider, although the emphasis is on frequency response methods rather than the more common time response approach.

It is gratifying that the stability and control properties of the hang glider as described by both Kroo and de Matteis are broadly in agreement with those described in the present work, which was undertaken quite independently.

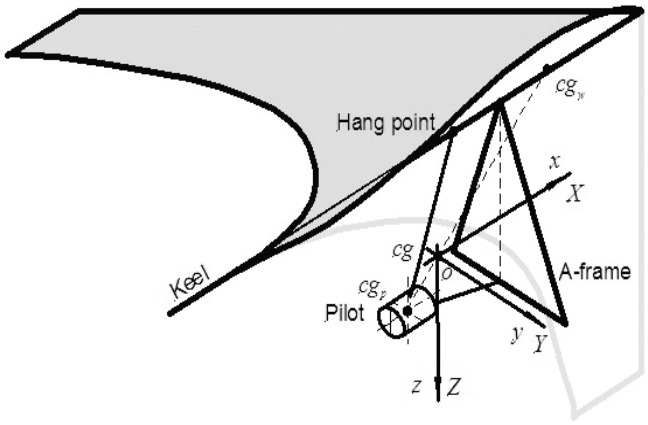

Figure 1. Hang glider body axis system.

3.0 THE HANG GLIDER MODEL

3.1 Axis system and geometry

The hang glider is defined as a pilot suspended below a wing by the hang strap, in such a way that the pilot may move with respect to the wing, subject to the constraint of the hang strap. The geometry of this arrangement is illustrated in Fig. 1. The hang strap is attached to the central keel tube of the wing at the hang point and in normal operation it is usual to assume that the hang strap behaves as a rigid bar. It is convenient to define the keel as the longitudinal chordwise reference axis of the wing since it is the main structural member and lies in the plane of symmetry. In order to control the hang glider the pilot positions himself relative to the wing by 'pushing and pulling' on the control bar which is the lower spanwise member of the triangular A-frame, or control frame. Any trimmed flight condition is therefore determined solely by the unique geometry of the pilot-wing combination.

For the purposes of mathematical modelling, an orthogonal body fixed axis system is defined (*oxyz*) with origin coincident with the vehicle *cg* and *ox* axis parallel to the keel axis. The axes are arranged as for conventional aeroplanes such that in trimmed equilibrium the axes (*oxz*) define the plane of symmetry. Since the mass of the hang glider may be represented separately by the wing mass m_w and pilot mass m_p, the *cg* lies on a line joining the *cg* of the wing with the *cg* of the pilot as indicated in Fig. 1. The location of the centre of gravity of the wing *cgw* is defined by co-ordinates (x_w, y_w, z_w) and the location of the centre of gravity of the pilot *cgp* is defined by co-ordinates (x_p, y_p, z_p). Hence the *cg* position relative to the aerodynamic centre of the wing as well as the moments and products of inertia about the system axes are different for each trim state. The approach adopted assumes the hang glider to be rigid in its trim geometry and considers small perturbation motion about the trim state. Thus the mass matrix of the equations of motion is constant for a given trim condition but differs from one trim condition to the next. With the system thus defined, the small perturbation equations of motion about the system centre of gravity were developed by Spottiswoode[9] using the classical methods and notational style described by Cook[13].

The longitudinal geometry is shown in greater detail in Fig. 2. In steady straight gliding flight with velocity V_0, the pitch attitude θ is defined as shown and hence body incidence α and flight path angle γ are also defined. For simplicity the pilot is modelled as a cylinder having a uniform mass distribution and with its axis of symmetry parallel to the keel reference. The longitudinal control angle δ is defined as the angle between the hang strap and a line parallel to the (*oz*) axis at the hang point. The axial force *X*, normal force *Z* and pitching moment *M* are also indicated in Fig. 2.

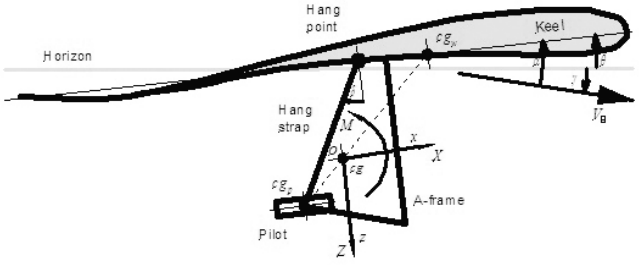

Figure 2. Longitudinal reference geometry.

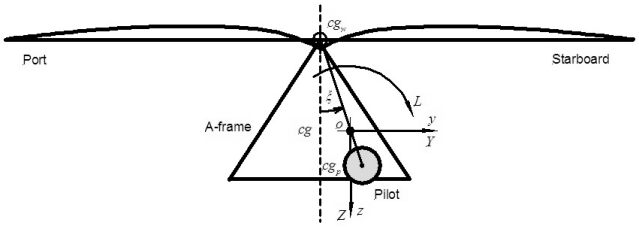

Figure 3. Lateral reference geometry.

Similarly, the lateral geometry is shown in Fig. 3. However, in order to show the lateral control angle ξ, the pilot mass is offset from the centre line, which would be representative of the instantaneous geometry at the commencement of a turn to starboard. The lateral control angle ξ is defined as the angle between the hang strap and a line parallel to the (oz) axis at the hang point. In steady straight trimmed flight the *cg* of the pilot is in the plane of symmetry and ξ = 0. Note that the orientation of the ($oxyz$) axes remains fixed with respect to the wing. The lateral side force Y, normal force Z and rolling moment L are also indicated in Fig. 3. In the following analytical development great care is required to avoid notational confusion and it should be noted that the use of most familiar symbols is context dependent.

3.2 Inertial equations

Spottiswoode[9] developed the small perturbation equations of motion from first principles, as a two mass multi-body system. However, since the origin of the axis system is coincident with the cg the equations simplify to the familiar form,

$$\begin{aligned} m\left(\dot{u}+qW_e\right) &= X = X_a + X_g \\ m\left(\dot{v}-pW_e+rU_e\right) &= Y = Y_a + Y_g \\ m\left(\dot{w}-qU_e\right) &= Z = Z_a + Z_g \\ I_x\dot{p}-I_{xz}\dot{r} &= L = L_a + L_g \\ I_y\dot{q} &= M = M_a + M_g \\ I_z\dot{r}-I_{xz}\dot{p} &= N = N_a + N_g \end{aligned} \qquad \ldots (1)$$

where the usual aircraft assumptions apply and the notation has the usual meaning. Further, the mass and inertia terms are each assumed to comprise the sum of the wing and pilot contributions referred to the axis system and since a symmetric airframe is assumed this reduces to the same form as the inertial equations of motion for a conventional aircraft. A significant difference for the hang glider application is that the inertias in Equations (1) are those of the coupled wing-pilot system, they vary with trim state, and therefore they must be

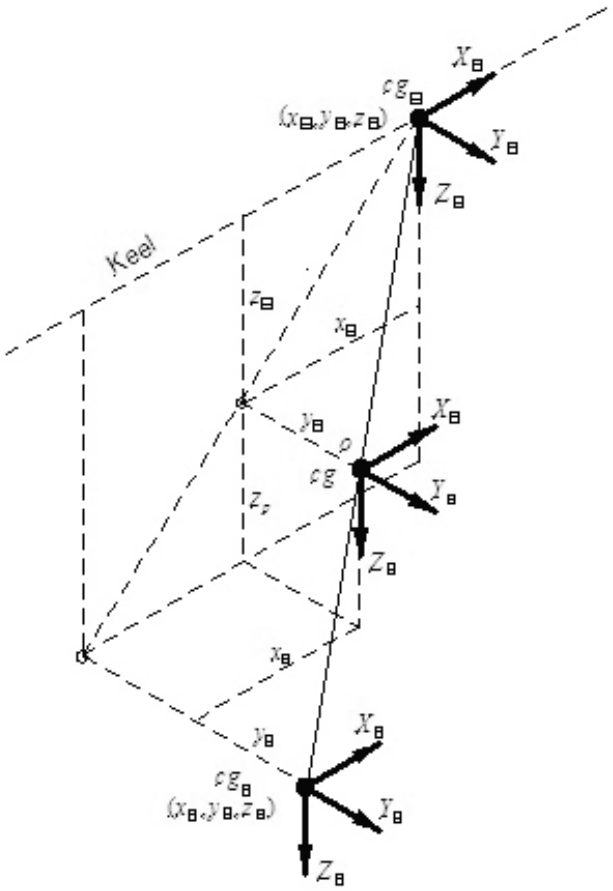

Figure 4. Axes systems geometry.

calculated for each flight case. The terms on the right hand side of Equations (1) allow for the aerodynamic and gravitational contributions to the forces and moments respectively. Contributions due to *cg* shift control are implicit in the aerodynamic model.

3.3 Gravity forces and moments

Again, Spottiswoode[9] developed expressions for the gravitational force and moment contributions to the equations of motion assuming a two mass multi-body system. As before, since the origin of axes is coincident with the *cg*, the expressions simplify to the familiar small perturbation form. In the notation of Cook[13],

$$\begin{aligned} X_g &= -mg\left(\mathrm{Sin}\theta_e + \theta\mathrm{Cos}\theta_e\right) \\ Y_g &= mg\left(\psi\mathrm{Sin}\theta_e + \phi\mathrm{Cos}\theta_e\right) \\ Z_g &= -mg\left(\theta\mathrm{Sin}\theta_e - \mathrm{Cos}\theta_e\right) \\ L_g &= M_g = N_g = 0 \end{aligned} \qquad \ldots (2)$$

and the total mass is given by,

$$m = m_w + m_p \qquad \ldots (3)$$

3.4 Aerodynamic forces and moments

The total aerodynamic force and moment components acting on the hang glider comprise the sum of wing and pilot contributions referred to the centre of gravity. The wing and pilot aerodynamic

force and moment components are defined with respect to their local centres of gravity and Fig. 4 shows a general arrangement of the local axes and force geometry of the hang glider. Moments are not shown in the interests of clarity. Thus, referring the local forces and moments for the wing and pilot to the hang glider centre of gravity,

$$
\begin{aligned}
X_a &= X_w + X_p \\
Y_a &= Y_w + Y_p \\
Z_a &= Z_w + Z_p \\
L_a &= (L_w + y_w Z_w - z_w Y_w) + (L_p + y_p Z_p - z_p Y_p) \\
M_a &= (M_w - x_w Z_w + z_w X_w) + (M_p - x_p Z_p + z_p X_p) \\
N_a &= (N_w + x_w Y_w - y_w X_w) + (N_p + x_p Y_p - y_p X_p)
\end{aligned}
\qquad \ldots (4)
$$

Now the aerodynamic force and moment components acting at the *cg* of the hang glider comprise steady trim and unsteady, or perturbation, contributions. Thus Equations (4) may be written alternatively,

$$
\begin{aligned}
X_a &= (X_{w_e} + X_{p_e}) + (X_w + X_p) \\
Y_a &= (Y_{w_e} + Y_{p_e}) + (Y_w + Y_p) \\
Z_a &= (Z_{w_e} + Z_{p_e}) + (Z_w + Z_p) \\
L_a &= (L_{w_e} + y_w Z_{w_e} - z_w Y_{w_e}) + (L_{p_e} + y_p Z_{p_e} - z_p Y_{p_e}) \\
&\quad + (L_w + y_w Z_w - z_w Y_w) + (L_p + y_p Z_p - z_p Y_p) \\
M_a &= (M_{w_e} - x_w Z_{w_e} + z_w X_{w_e}) + (M_{p_e} - x_p Z_{p_e} + z_p X_{p_e}) \\
&\quad + (M_w - x_w Z_w + z_w X_w) + (M_p - x_p Z_p + z_p X_p) \\
N_a &= (N_{w_e} + x_w Y_{w_e} - y_w X_{w_e}) + (N_{p_e} + x_p Y_{p_e} - y_p X_{p_e}) \\
&\quad + (N_w + x_w Y_w - y_w X_w) + (N_p + x_p Y_p - y_p X_p)
\end{aligned}
\qquad \ldots (5)
$$

where the subscripts *e*, *p* and *w* refer to steady trim equilibrium, pilot contribution and wing contribution respectively. In steady trimmed symmetric equilibrium flight,

$$
\begin{aligned}
Y_{w_e} = L_{w_e} = N_{w_e} &= 0 \\
Y_{p_e} = L_{p_e} = N_{p_e} &= 0
\end{aligned}
\qquad \ldots (6)
$$

Thus Equations (5) simplify to,

$$
\begin{aligned}
X_a &= (X_{w_e} + X_{p_e}) + (X_w + X_p) \\
Y_a &= (Y_w + Y_p) \\
Z_a &= (Z_{w_e} + Z_{p_e}) + (Z_w + Z_p) \\
L_a &= (y_w Z_{w_e} + y_p Z_{p_e}) + (L_w + y_w Z_w - z_w Y_w) \\
&\quad + (L_p + y_p Z_p - z_p Y_p) \\
M_a &= (M_{w_e} - x_{w_e} Z_{w_e} + z_{w_e} X_{w_e}) \\
&\quad + (M_{p_e} - x_{p_e} Z_{p_e} + z_{p_e} X_{p_e}) \\
&\quad + (M_w - x_w Z_w + z_w X_w) \\
&\quad + (M_p - x_p Z_p + z_p X_p) \\
N_a &= (-y_w X_{w_e} - y_p X_{p_e}) + (N_w + x_w Y_w - y_w X_w) \\
&\quad + (N_p + x_p Y_p - y_p X_p)
\end{aligned}
\qquad \ldots (7)
$$

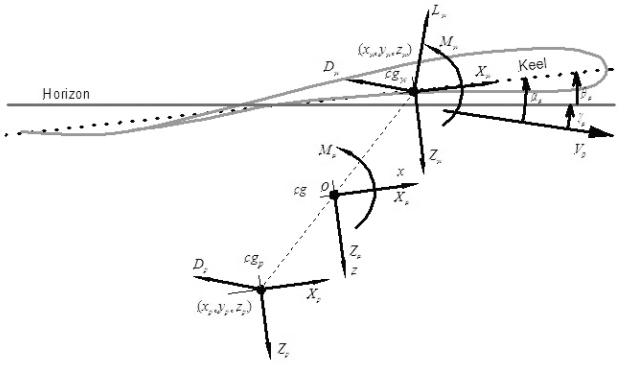

Figure 5. Symmetric trim geometry.

3.5 Steady equilibrium forces and moments

The symmetric trim geometry applying in trimmed equilibrium flight is shown in Fig. 5 in which the wing lift L_w (not to be confused with rolling moment), drag D_w and pitching moment M_{0_w} are referred to the wing centre of gravity cg_w, and the pilot drag D_p acts at the centre of gravity of the pilot cg_p. It has been shown by Kilkenny[4] that the only significant steady aerodynamic property of the pilot is drag and that drag coefficient remains nominally constant for all flight conditions. Thus, with reference to Fig. 5, the steady aerodynamic forces and moments referred to the centre of gravity of the hang glider may be written,

$$
\begin{aligned}
(X_{w_e} + X_{p_e}) &= L_w \sin\alpha_e - (D_w + D_p)\cos\alpha_e \\
(Z_{w_e} + Z_{p_e}) &= -L_w \cos\alpha_e - (D_w + D_p)\sin\alpha_e \\
(Y_{w_e} + Y_{p_e}) &= 0 \\
(y_w Z_{w_e} + y_p Z_{p_e}) &= -y_w \begin{pmatrix} L_w \cos\alpha_e \\ +D_w \sin\alpha_e \end{pmatrix} - y_p D_p \sin\alpha_e \\
\begin{pmatrix} (M_{w_e} - x_w Z_{w_e} + z_w X_{w_e}) \\ +(M_{p_e} - x_p Z_{p_e} + z_p X_{p_e}) \end{pmatrix} &= M_{0_w} \\
&\quad + \begin{pmatrix} (x_w D_w + z_w L_w + x_p D_p)\sin\alpha_e \\ +(x_w L_w - z_w D_w - z_p D_p)\cos\alpha_e \end{pmatrix} \\
(-y_w X_{w_e} - y_p X_{p_e}) &= -y_w \begin{pmatrix} L_w \sin\alpha_e \\ -D_w \cos\alpha_e \end{pmatrix} + y_p D_p \cos\alpha_e
\end{aligned}
\qquad \ldots (8)
$$

3.6 Unsteady perturbation forces and moments

The aerodynamic forces and moments arising as a result of a perturbation in the motion variables may be expressed in terms of classical stability and control derivatives. Assuming the perturbation to be small and that the equations of motion may be decoupled, consider the wing contribution to Equations (7). The unsteady aerodynamic forces and moments due to a small perturbation about trim, referred

to local body axes with origin at the wing centre of gravity cg_w, may be expressed in terms of stability derivatives in the usual way. Assuming decoupled motion and since the vehicle is tailless the downwash lag ($\dot{w}$) derivatives may be neglected. Whence,

$$
\begin{aligned}
X_w &= \overset{\circ}{X}_{u_w} u_w + \overset{\circ}{X}_{w_w} w_w + \overset{\circ}{X}_{q_w} q_w \\
Y_w &= \overset{\circ}{Y}_{v_w} v_w + \overset{\circ}{Y}_{p_w} p_w + \overset{\circ}{Y}_{r_w} r_w \\
Z_w &= \overset{\circ}{Z}_{u_w} u_w + \overset{\circ}{Z}_{w_w} w_w + \overset{\circ}{Z}_{q_w} q_w \\
L_w &= \overset{\circ}{L}_{v_w} v_w + \overset{\circ}{L}_{p_w} p_w + \overset{\circ}{L}_{r_w} r_w \\
M_w &= \overset{\circ}{M}_{u_w} u_w + \overset{\circ}{M}_{w_w} w_w + \overset{\circ}{M}_{q_w} q_w \\
N_w &= \overset{\circ}{N}_{v_w} v_w + \overset{\circ}{N}_{p_w} p_w + \overset{\circ}{N}_{r_w} r_w
\end{aligned}
\qquad \ldots (9)
$$

Now the perturbation velocities at cg_w may be expressed in terms of the perturbation velocities at the hang glider cg as follows,

$$
\begin{aligned}
u_w &= u + qz_w - ry_w = u + qz_w \qquad & p_w &= p \\
v_w &= v - pz_w + rx_w & q_w &= q \\
w_w &= w - qx_w + py_w = w - qx_w & r_w &= r
\end{aligned}
\qquad \ldots (10)
$$

For small perturbation motion, the aerodynamic forces and moments given by Equations (9) may be referred to the hang glider cg,

$$
\begin{aligned}
X_w &= \overset{\circ}{X}_u u + \overset{\circ}{X}_w w + \left(\overset{\circ}{X}_q + z_w \overset{\circ}{X}_u - x_w \overset{\circ}{X}_w \right) q \\
&= \overset{\circ}{X}_{u_w} u + \overset{\circ}{X}_{w_w} w + \left(z_w \overset{\circ}{X}_{u_w} - x_w \overset{\circ}{X}_{w_w} \right) q \\
Y_w &= \overset{\circ}{Y}_{v_w} v + \left(\overset{\circ}{Y}_{p_w} - z_w \overset{\circ}{Y}_{v_w} \right) p + \left(\overset{\circ}{Y}_{r_w} + x_w \overset{\circ}{Y}_{v_w} \right) r \\
&= \overset{\circ}{Y}_{v_w} v - z_w \overset{\circ}{Y}_{v_w} p + x_w \overset{\circ}{Y}_{v_w} r \\
Z_w &= \overset{\circ}{Z}_{u_w} u + \overset{\circ}{Z}_{w_w} w + \left(\overset{\circ}{Z}_{q_w} + z_w \overset{\circ}{Z}_{u_w} - x_w \overset{\circ}{Z}_{w_w} \right) q \\
L_w &= \overset{\circ}{L}_{v_w} v + \left(\overset{\circ}{L}_{p_w} - z_w \overset{\circ}{L}_{v_w} \right) p + \left(\overset{\circ}{L}_{r_w} + x_w \overset{\circ}{L}_{v_w} \right) r \\
M_w &= \overset{\circ}{M}_{u_w} u + \overset{\circ}{M}_{w_w} w + \left(\overset{\circ}{M}_{q_w} + z_w \overset{\circ}{M}_{u_w} - x_w \overset{\circ}{M}_{w_w} \right) q \\
N_w &= \overset{\circ}{N}_{v_w} v + \left(\overset{\circ}{N}_{p_w} - z_w \overset{\circ}{N}_{v_w} \right) p + \left(\overset{\circ}{N}_{r_w} + x_w \overset{\circ}{N}_{v_w} \right) r
\end{aligned}
\qquad \ldots (11)
$$

when it is assumed that $\overset{\circ}{X}_{q_w} = \overset{\circ}{Y}_{p_w} = \overset{\circ}{Y}_{r_w} \cong 0$.

Consider secondly the pilot contribution to Equations (7). Assuming that the pilot aerodynamics can also be expressed in terms of body referenced derivatives, then the contributions can be written in the same format as Equations (11). Since the pilot is modelled as a cylinder, Spottiswoode[9] has shown that the following derivatives are negligible,

$$
\begin{aligned}
&\overset{\circ}{X}_{q_p} = \overset{\circ}{Z}_{q_p} = 0 \qquad && \overset{\circ}{M}_{u_p} = \overset{\circ}{M}_{w_p} = 0 \\
&\overset{\circ}{Y}_{p_p} = \overset{\circ}{Y}_{r_p} = 0 && \overset{\circ}{L}_{v_p} = \overset{\circ}{L}_{p_p} = \overset{\circ}{L}_{r_p} = 0 \\
& && \overset{\circ}{N}_{v_p} = \overset{\circ}{N}_{p_p} = 0
\end{aligned}
$$

Whence,

$$
\begin{aligned}
X_p &= \overset{\circ}{X}_{u_p} u + \overset{\circ}{X}_{w_p} w + \left(z_p \overset{\circ}{X}_{u_p} - x_p \overset{\circ}{X}_{w_p} \right) q \qquad & L_p &= 0 \\
Y_p &= \overset{\circ}{Y}_{v_p} v - z_p \overset{\circ}{Y}_{v_p} p + x_p \overset{\circ}{Y}_{v_p} r & M_p &= \overset{\circ}{M}_{q_p} q \\
Z_p &= \overset{\circ}{Z}_{u_p} u + \overset{\circ}{Z}_{w_p} w + \left(z_p \overset{\circ}{Z}_{u_p} - x_p \overset{\circ}{Z}_{w_p} \right) q & N_p &= \overset{\circ}{N}_{r_p} r
\end{aligned}
\qquad \ldots (12)
$$

3.7 Total aerodynamic forces and moments

The total aerodynamic force and moment components referred to the cg are given by Equations (7) and these may be expressed in terms of stability derivatives by substitution of Equations (8), (11) and (12) as follows.

$$
\begin{aligned}
X_a &= L_w \text{Sin}\, \alpha_e - \left(D_w + D_p \right) \text{Cos}\, \alpha_e \\
&\quad + \left(\overset{\circ}{X}_{u_w} + \overset{\circ}{X}_{u_p} \right) u + \left(\overset{\circ}{X}_{w_w} + \overset{\circ}{X}_{w_p} \right) w \\
&\quad + \left(z_w \overset{\circ}{X}_{u_w} + z_p \overset{\circ}{X}_{u_p} - x_w \overset{\circ}{X}_{w_w} - x_p \overset{\circ}{X}_{w_p} \right) q \\
Y_a &= \left(\overset{\circ}{Y}_{v_w} + \overset{\circ}{Y}_{v_p} \right) v - \left(z_w \overset{\circ}{Y}_{v_w} + z_p \overset{\circ}{Y}_{v_p} \right) p \\
&\quad + \left(x_w \overset{\circ}{Y}_{v_w} + x_p \overset{\circ}{Y}_{v_p} \right) r \\
Z_a &= -L_w \text{Cos}\, \alpha_e - \left(D_w + D_p \right) \text{Sin}\, \alpha_e \\
&\quad + \left(\overset{\circ}{Z}_{u_w} + \overset{\circ}{Z}_{u_p} \right) u + \left(\overset{\circ}{Z}_{w_w} + \overset{\circ}{Z}_{w_p} \right) w \\
&\quad + \left(\overset{\circ}{Z}_{q_w} + z_w \overset{\circ}{Z}_{u_w} + z_p \overset{\circ}{Z}_{u_p} - x_w \overset{\circ}{Z}_{w_w} - x_p \overset{\circ}{Z}_{w_p} \right) q \\
L_a &= -y_w \left(L_w \text{Cos}\, \alpha_e + D_w \text{Sin}\, \alpha_e \right) - y_p D_p \text{Sin}\, \alpha_e \\
&\quad + \left(y_w \overset{\circ}{Z}_{u_w} + y_p \overset{\circ}{Z}_{u_p} \right) u + \left(\overset{\circ}{L}_{v_w} - z_w \overset{\circ}{Y}_{v_w} - z_p \overset{\circ}{Y}_{v_p} \right) v \\
&\quad + \left(y_w \overset{\circ}{Z}_{w_w} + y_p \overset{\circ}{Z}_{w_p} \right) w \\
&\quad + \left(\overset{\circ}{L}_{p_w} - z_w \overset{\circ}{L}_{v_w} + z_w^2 \overset{\circ}{Y}_{v_w} + z_p^2 \overset{\circ}{Y}_{v_p} \right) p \\
&\quad + \left(\begin{array}{l} y_w \overset{\circ}{Z}_{q_w} + y_w z_w \overset{\circ}{Z}_{u_w} - y_w x_w \overset{\circ}{Z}_{w_w} \\ + y_p z_p \overset{\circ}{Z}_{u_p} - y_p x_p \overset{\circ}{Z}_{w_p} \end{array} \right) q \\
&\quad + \left(\overset{\circ}{L}_{r_w} + x_w \overset{\circ}{L}_{v_w} - z_w x_w \overset{\circ}{Y}_{v_w} - z_p x_p \overset{\circ}{Y}_{v_p} \right) r \\
M_a &= M_{0_w} + \left(x_w D_w + z_w L_w + x_p D_p \right) \text{Sin}\, \alpha_e \\
&\quad + \left(x_w L_w - z_w D_w - Z_p D_p \right) \text{Cos}\, \alpha_e \\
&\quad + \left(\overset{\circ}{M}_{u_w} - x_w \overset{\circ}{Z}_{u_w} + z_w \overset{\circ}{X}_{u_w} - x_p \overset{\circ}{Z}_{u_p} + z_p \overset{\circ}{X}_{u_p} \right) u \\
&\quad + \left(\overset{\circ}{M}_{w_w} - x_w \overset{\circ}{Z}_{w_w} + z_w \overset{\circ}{X}_{w_w} - x_p \overset{\circ}{Z}_{w_p} + z_p \overset{\circ}{X}_{w_p} \right) w
\end{aligned}
\qquad \ldots (13)
$$

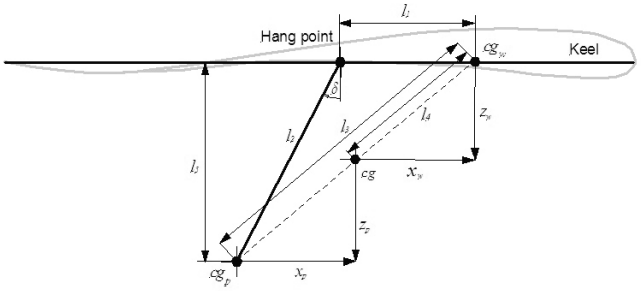

Figure 6. Longitudinal control geometry.

$$+\begin{pmatrix} \mathring{M}_{q_w}+\mathring{M}_{q_p}+z_w\mathring{M}_{u_w}-x_w\mathring{M}_{w_w} \\ -x_w\mathring{Z}_{q_w}-x_w z_w\mathring{Z}_{u_w}+x_w^2\mathring{Z}_{w_w} \\ +z_w^2\mathring{X}_{u_w}-x_w z_w\mathring{X}_{w_w}-x_p z_p\mathring{Z}_{u_p} \\ +x_p^2\mathring{Z}_{w_p}+z_p^2\mathring{X}_{u_p}-x_p z_p\mathring{X}_{w_p} \end{pmatrix} q$$

$$\begin{aligned} N_a = {} & -y_w\left(L_w\text{Sin}\,\alpha_e - D_w\text{Cos}\,\alpha_e\right)+y_p D_p\,\text{Cos}\,\alpha_e \\ & +\left(-y_w\mathring{X}_{u_w}-y_p\mathring{X}_{u_p}\right)u \\ & +\left(\mathring{N}_{v_w}+x_w\mathring{Y}_{v_w}+x_p\mathring{Y}_{v_p}\right)v+\left(-y_w\mathring{X}_{w_w}-y_p\mathring{X}_{w_p}\right)w \\ & +\left(\mathring{N}_{p_w}-z_w\mathring{N}_{v_w}-x_w z_w\mathring{Y}_{v_w}-x_p z_p\mathring{Y}_{v_p}\right)p \\ & +\left(-y_w z_w\mathring{X}_{u_w}+y_w x_w\mathring{X}_{w_w}-y_p z_p\mathring{X}_{u_p}+y_p x_p\mathring{X}_{w_p}\right)q \\ & +\left(\mathring{N}_{r_w}+\mathring{N}_{r_p}+x_w\mathring{N}_{v_w}+x_w^2\mathring{Y}_{v_w}+x_p^2\mathring{Y}_{v_p}\right)r \end{aligned}$$

If pilot control action causes the *cg* to move through (δ_x, δ_y, δ_z) then the local wing and pilot *cg* co-ordinates may be written,

$$\begin{aligned} x_w &= x_{w_e}+\delta x_w & x_p &= x_{p_e}+\delta x_p \\ y_w &= y_{w_e}+\delta y_w = \delta y_w & y_p &= y_{p_e}+\delta y_p = \delta y_p \\ z_w &= z_{w_e}+\delta z_w & z_p &= z_{p_e}+\delta z_p \end{aligned} \quad \ldots (14)$$

since $y_{we} = y_{pe} = 0$ when the hang glider is in trimmed equilibrium flight. Substituting Equations (14) into Equations (13) and recognising that the control inputs (δx_w, δy_w, δz_w) and (δx_p, δy_p, δz_p) are assumed small such that the products of small perturbation quantities may be neglected,

$$\begin{aligned} X_a = {} & L_w\text{Sin}\,\alpha_e-\left(D_w+D_p\right)\text{Cos}\,\alpha_e \\ & +\left(\mathring{X}_{u_w}+\mathring{X}_{u_p}\right)u+\left(\mathring{X}_{w_w}+\mathring{X}_{w_p}\right)w \\ & +\left(z_{w_e}\mathring{X}_{u_w}+z_{p_e}\mathring{X}_{u_p}-x_{w_e}\mathring{X}_{w_w}-x_{p_e}\mathring{X}_{w_p}\right)q \end{aligned} \quad \ldots (15)$$

$$Y_a = \left(\mathring{Y}_{v_w}+\mathring{Y}_{v_p}\right)v-\left(z_{w_e}\mathring{Y}_{v_w}+z_{p_e}\mathring{Y}_{v_p}\right)p+\left(x_{w_e}\mathring{Y}_{v_w}+x_{p_e}\mathring{Y}_{v_p}\right)r$$

$$\begin{aligned} Z_a = {} & -L_w\text{Cos}\,\alpha_e-\left(D_w+D_p\right)\text{Sin}\,\alpha_e \\ & +\left(\mathring{Z}_{u_w}+\mathring{Z}_{u_p}\right)u+\left(\mathring{Z}_{w_w}+\mathring{Z}_{w_p}\right)w \\ & +\left(\mathring{Z}_{q_w}+z_{w_e}\mathring{Z}_{u_w}+z_{p_e}\mathring{Z}_{u_p}-x_{w_e}\mathring{Z}_{w_w}-x_{p_e}\mathring{Z}_{w_p}\right)q \end{aligned}$$

$$\begin{aligned} L_a = {} & \left(\mathring{L}_{v_w}-z_{w_e}\mathring{Y}_{v_w}-z_{p_e}\mathring{Y}_{v_p}\right)v \\ & +\left(\mathring{L}_{p_w}-z_{w_e}\left(\mathring{L}_{v_w}-z_{w_e}\mathring{Y}_{v_w}\right)+z_{p_e}^2\mathring{Y}_{v_p}\right)p \\ & +\left(\mathring{L}_{r_w}+x_{w_e}\left(\mathring{L}_{v_w}-z_{w_e}\mathring{Y}_{v_w}\right)-z_{p_e}x_{p_e}\mathring{Y}_{v_p}\right)r \\ & -\left(L_w\text{Cos}\,\alpha_e+D_w\text{Sin}\,\alpha_e\right)\delta y_w-D_p\,\text{Sin}\,\alpha_e\,\delta y_p \end{aligned}$$

$$\begin{aligned} M_a = {} & M_{0_w}+\left(z_{w_e}L_w+x_{w_e}D_w+x_{p_e}D_p\right)\text{Sin}\,\alpha_e \\ & +\left(x_{w_e}L_w-z_{w_e}D_w-z_{p_e}D_p\right)\text{Cos}\,\alpha_e \\ & +\left(\mathring{M}_{u_w}-x_{w_e}\mathring{Z}_{u_w}+z_{w_e}\mathring{X}_{u_w}-x_{p_e}\mathring{Z}_{u_p}+z_{p_e}\mathring{X}_{u_p}\right)u \\ & +\left(\mathring{M}_{w_w}-x_{w_e}\mathring{Z}_{w_w}+z_{w_e}\mathring{X}_{w_w}-x_{p_e}\mathring{Z}_{w_p}+z_{p_e}\mathring{X}_{w_p}\right)w \\ & +\begin{pmatrix} \mathring{M}_{q_w}+\mathring{M}_{q_p}+z_{w_e}\mathring{M}_{u_w}-x_{w_e}\left(\mathring{M}_{w_w}+\mathring{Z}_{q_w}\right) \\ -x_{w_e}z_{w_e}\left(\mathring{Z}_{u_w}+\mathring{X}_{w_w}\right) \\ +x_{w_e}^2\mathring{Z}_{w_w}+z_{w_e}^2\mathring{X}_{u_w}-x_{p_e}z_{p_e}\left(\mathring{Z}_{u_p}+\mathring{X}_{w_p}\right) \\ +x_{p_e}^2\mathring{Z}_{w_p}+z_{p_e}^2\mathring{X}_{u_p} \end{pmatrix} q \\ & +\left(L_w\text{Cos}\,\alpha_e+D_w\text{Sin}\,\alpha_e\right)\delta x_w+D_p\,\text{Sin}\,\alpha_e\,\delta x_p \\ & +\left(L_w\text{Sin}\,\alpha_e-D_w\text{Cos}\,\alpha_e\right)\delta z_w-D_p\,\text{Cos}\,\alpha_e\,\delta z_p \end{aligned}$$

$$\begin{aligned} N_a = {} & \left(\mathring{N}_{v_w}+x_{w_e}\mathring{Y}_{v_w}+x_{p_e}\mathring{Y}_{v_p}\right)v \\ & +\left(\mathring{N}_{p_w}-z_{w_e}\left(\mathring{N}_{v_w}+x_{w_e}\mathring{Y}_{v_w}\right)-x_{p_e}z_{p_e}\mathring{Y}_{v_p}\right)p \\ & +\left(\mathring{N}_{r_w}+\mathring{N}_{r_p}+x_{w_e}\left(\mathring{N}_{v_w}+x_{w_e}\mathring{Y}_{v_w}\right)+x_{p_e}^2\mathring{Y}_{v_p}\right)r \\ & -\left(L_w\text{Sin}\,\alpha_e-D_w\text{Cos}\,\alpha_e\right)\delta y_w \\ & +D_p\text{Cos}\,\alpha_e\delta y_p \end{aligned}$$

3.8 Control geometry

Since control commands are described by the longitudinal and lateral control angles, δ and ξ respectively, it is more convenient to express the pilot demanded *cg* shift in terms of these variables together with other known geometric parameters. The longitudinal control geometry is shown on Fig. 6, where l_1 is the distance from cg_w to the hang point and l_2 is the length of the hang strap.

With reference to Fig. 6 and observing the co-ordinate sign convention it is seen that,

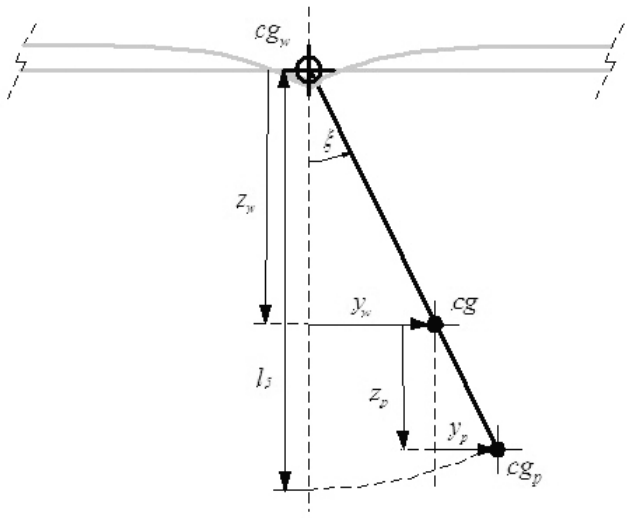

Figure 7(a). Lateral control geometry – forward view. Instantaneous roll command.

$$x_w - x_p = l_1 + l_2 \text{ Sin } \delta$$
$$z_p - z_w = l_5 = l_2 \text{Cos } \delta \quad \ldots (16)$$

and it is easily shown that,

$$\frac{x_p}{x_w} = \frac{z_p}{z_w} = 1 - \frac{l_3}{l_4} \equiv 1 - \frac{m}{m_p} = -\frac{m_w}{m_p} \quad \ldots (17)$$

Solving Equations (16) and (17),

$$x_w = \frac{m_p}{m}(l_1 + l_2 \text{ Sin } \delta) \qquad z_w = -\frac{m_p}{m} l_2 \text{Cos } \delta$$
$$x_p = -\frac{m_w}{m}(l_1 + l_2 \text{ Sin } \delta) \quad z_p = \frac{m_w}{m} l_2 \text{Cos } \delta \quad \ldots (18)$$

The instantaneous lateral control geometry following a roll command is shown in Fig. 7(a). However, the roll couple created by the lift vector and pilot weight will cause the hang glider to immediately adopt a roll attitude closer to that assumed in Fig. 7(b). In practice the hang strap is unlikely to be exactly vertical since additional rolling moments will be created as the turning motion becomes established. Once the pilot has achieved his desired bank angle a balanced turn without sideslip is maintained by returning the control angle ξ to zero. Provided the hang glider is laterally stable, it will remain in the turn until the pilot takes the appropriate recovery action. The lateral control geometry is the same in both cases shown in Fig. 7 and it is easily shown that,

$$y_w = -l_5 \frac{m_p}{m} \text{Sin } \xi \equiv -l_2 \frac{m_p}{m} \text{Cos } \delta \text{Sin } \xi$$
$$y_p = l_5 \frac{m_w}{m} \text{Sin } \xi \equiv l_2 \frac{m_w}{m} \text{Cos } \delta \text{Sin } \xi \quad \ldots (19)$$
$$z_w = -l_2 \frac{m_p}{m} \text{Cos } \delta \text{ Cos } \xi$$
$$z_p = l_2 \frac{m_w}{m} \text{Cos } \delta \text{ Cos } \xi$$

If the control angles are assumed to comprise a steady equilibrium trim component and a small perturbation control component then it

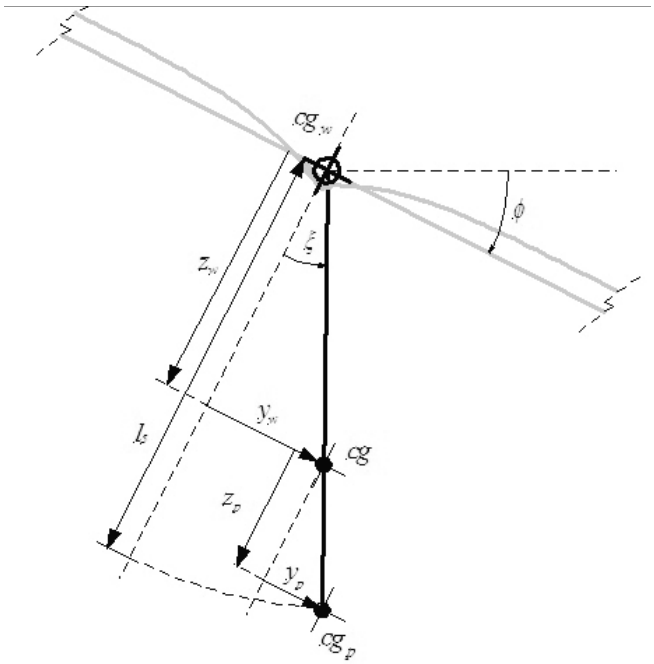

Figure 7(b). Lateral control geometry – forward view. Established roll command.

is convenient to write,

$$\delta = \delta_e + \delta$$
$$\xi = \xi_e + \xi \quad \ldots (20)$$

Substituting the expressions (14) and (20) into Equations (18) and (19), making the appropriate small angle approximations and noting that in symmetric trim equilibrium,

$$y_{w_e} = y_{p_e} = \xi_e = 0$$

then the control terms may be written,

$$x_{w_e} + \delta x_w = \frac{m_p}{m}\left((l_1 + l_2 \text{ Sin } \delta_e) + (l_2 \text{Cos } \delta_e)\delta\right)$$
$$x_{p_e} + \delta x_p = -\frac{m_w}{m}\left((l_1 + l_2 \text{ Sin } \delta_e) + (l_2 \text{Cos } \delta_e)\delta\right)$$
$$z_{w_e} + \delta z_w = -\frac{m_p}{m} l_2 \left(\text{ Sin } \delta_e - (\text{Cos } \delta_e)\delta\right)$$
$$z_{p_e} + \delta z_p = \frac{m_w}{m} l_2 \left(\text{ Sin } \delta_e - (\text{Cos } \delta_e)\delta\right) \quad \ldots (21)$$
$$\delta y_w = -\frac{m_p}{m} l_2 (\text{Cos } \delta_e)\xi$$
$$\delta y_p = \frac{m_w}{m} l_2 (\text{Cos } \delta_e)\xi$$

Thus the small perturbation control terms may be summarised,

$$\begin{bmatrix}\delta x_w\\ \delta z_w\\ \delta x_p\\ \delta z_p\end{bmatrix}=\begin{bmatrix}\frac{m_p}{m}l_2\text{Cos }\delta_e\\ \frac{m_p}{m}l_2\text{ Sin }\delta_e\\ -\frac{m_w}{m}l_2\text{Cos }\delta_e\\ -\frac{m_w}{m}l_2\text{ Sin }\delta_e\end{bmatrix}\delta \qquad \ldots (22)$$

$$\begin{bmatrix}\delta y_w\\ \delta y_p\end{bmatrix}=\begin{bmatrix}-\frac{m_p}{m}l_2\cos\delta_e\\ \frac{m_w}{m}l_2\cos\delta_e\end{bmatrix}\xi$$

and the symmetric trim equilibrium control terms may be summarised,

$$\begin{aligned}x_{w_e}&=\frac{m_p}{m}(l_1+l_2\text{ Sin }\delta_e)\\ z_{w_e}&=-\frac{m_p}{m}l_2\text{ Sin }\delta_e\\ x_{p_e}&=-\frac{m_w}{m}(l_1+l_2\text{ Sin }\delta_e)\\ z_{p_e}&=\frac{m_w}{m}l_2\text{ Sin }\delta_e\\ y_{w_e}&=y_{p_e}=0\end{aligned} \qquad \ldots (23)$$

3.9 Simplified aerodynamic model

The aerodynamic model represented by Equations (15) may be simplified by rewriting in terms of equivalent aerodynamic derivatives, referred to body axes, and in terms of the control angles δ, ξ.

$$\begin{aligned}X_a&=L_w\text{ Sin }\alpha_e-(D_w+D_p)\text{Cos }\alpha_e\\ &\quad+\overset{\circ}{X}^*_u u+\overset{\circ}{X}^*_w w+\overset{\circ}{X}^*_q q\\ Y_a&=\overset{\circ}{Y}^*_v v+\overset{\circ}{Y}^*_p p+\overset{\circ}{Y}^*_r r\\ Z_a&=-L_w\text{Cos }\alpha_e-(D_w+D_p)\text{ Sin }\alpha_e\\ &\quad+\overset{\circ}{Z}^*_u u+\overset{\circ}{Z}^*_w w+\overset{\circ}{Z}^*_q q\\ L_a&=\overset{\circ}{L}^*_v v+\overset{\circ}{L}^*_p p+\overset{\circ}{L}^*_r r+\overset{\circ}{L}^*_\xi\xi\\ M_a&=M_{0_w}+(z_{w_e}L_w+x_{w_e}D_w+x_{p_e}D_p)\text{ Sin }\alpha_e\\ &\quad+(x_{w_e}L_w-z_{w_e}D_w-z_{p_e}D_p)\text{Cos }\alpha_e\\ &\quad+\overset{\circ}{M}^*_u u+\overset{\circ}{M}^*_w w+\overset{\circ}{M}^*_q q+\overset{\circ}{M}^*_\delta\delta\\ N_a&=\overset{\circ}{N}^*_v v+\overset{\circ}{N}^*_p p+\overset{\circ}{N}^*_r r+\overset{\circ}{N}^*_\xi\xi\end{aligned} \qquad \ldots (24)$$

where (*) signifies an equivalent aerodynamic stability or control derivative, referred to body axes with origin at the *cg*. The dimensional equivalent aerodynamic stability derivatives are defined by the corresponding expressions in Table 1.

The equivalent control derivatives are determined by substituting the *cg* shift control variables, Equations (22), into Equations (15) and comparing the relevant terms with those in Equations (24) to obtain,

$$\begin{aligned}\overset{\circ}{M}^*_\delta&=\frac{l_2}{m}\text{Cos }\delta_e\begin{pmatrix}m_pL_w\text{Cos }(\delta_e-\alpha_e)\\ +(m_pD_w-m_wD_p)\text{ Sin }(\delta_e-\alpha_e)\end{pmatrix}\\ \overset{\circ}{L}^*_\xi&=\frac{l_2}{m}\text{Cos }\delta_e\begin{pmatrix}m_pL_w\text{Cos }\alpha_e\\ +(m_pD_w-m_wD_p)\text{ Sin }\alpha_e\end{pmatrix}\\ \overset{\circ}{N}^*_\xi&=\frac{l_2}{m}\text{Cos }\delta_e\begin{pmatrix}m_pL_w\text{ Sin }\alpha_e\\ -(m_pD_w-m_wD_p)\text{Cos }\alpha_e\end{pmatrix}\end{aligned} \qquad \ldots (25)$$

Now the roll and yaw control derivatives in Equations (25) refer to the instantaneous condition immediately following application of the roll command ξ as defined by the geometry shown in Fig. 7(a). If the roll command is held in the normal way, the roll couple created by the lift vector and pilot weight will cause the hang glider to immediately adopt the roll attitude illustrated in Fig. 7(b) while the turn becomes established, and in the absence of any other aerodynamic contributions. In this condition the drag moment contributions to the roll control derivative $\overset{\circ}{L}^*_\xi$ become zero and the yaw control derivative $\overset{\circ}{N}^*_\xi$ becomes completely zero. Thus the effective equivalent control derivatives are summarised in Table 2.

The linear equations of motion follow when the gravitational terms, Equations (2), and the aerodynamic terms, Equations (24), are substituted into Equations (1),

$$\begin{aligned}m\dot{u}&=L_w\text{ Sin }\alpha_e-(D_w+D_p)\text{Cos }\alpha_e-mg\text{ Sin }\theta_e\\ &\quad+\overset{\circ}{X}^*_u u+\overset{\circ}{X}^*_w w+\left(\overset{\circ}{X}^*_q-W_e\right)q-(mg\text{Cos }\theta_e)\theta\\ m\dot{v}&=\overset{\circ}{Y}^*_v v+\left(\overset{\circ}{Y}^*_p+W_e\right)p+\left(\overset{\circ}{Y}^*_r-U_e\right)r\\ &\quad+(mg\text{Cos }\theta_e)\phi+(mg\text{ Sin }\theta_e)\psi\\ m\dot{w}&=mg\text{Cos }\theta_e-L_w\cos\alpha_e-(D_w+D_p)\text{ Sin }\alpha_e\\ &\quad+\overset{\circ}{Z}^*_u u+\overset{\circ}{Z}^*_w w+\left(\overset{\circ}{Z}^*_q+U_e\right)q-(mg\text{ Sin }\theta_e)\theta\\ I_x\dot{p}-I_{xz}\dot{r}&=\overset{\circ}{L}^*_v v+\overset{\circ}{L}^*_p p+\overset{\circ}{L}^*_r r+\overset{\circ}{L}^*_\xi\xi\\ I_y\dot{q}&=M_{0_w}+(z_{w_e}L_w+x_{w_e}D_w+x_{p_e}D_p)\text{ Sin }\alpha_e\\ &\quad+(x_{w_e}L_w-z_{w_e}D_w-z_{p_e}D_p)\text{Cos }\alpha_e\\ &\quad+\overset{\circ}{M}^*_u u+\overset{\circ}{M}^*_w w+\overset{\circ}{M}^*_q q+\overset{\circ}{M}^*_\delta\delta\\ I_z\dot{r}-I_{xz}\dot{p}&=\overset{\circ}{N}^*_v v+\overset{\circ}{N}^*_p p+\overset{\circ}{N}^*_r r+\overset{\circ}{N}^*_\xi\xi\end{aligned} \qquad \ldots (26)$$

3.10 The trim equations

In trim the perturbation variables are zero and Equations (26) reduce to the simple equilibrium equations,

$$\begin{aligned}X_e&=L_w\text{ Sin }\alpha_e-(D_w+D_p)\text{Cos }\alpha_e-mg\text{ Sin }\theta_e=0\\ Y_e&=0\\ Z_e&=mg\text{Cos }\theta_e-L_w\text{Cos }\alpha_e-(D_w+D_p)\text{ Sin }\alpha_e=0\\ L_e&=0\end{aligned} \qquad \ldots (27)$$

Table 1
Equivalent aerodynamic stability derivatives
Referred to body axes

$\overset{\circ}{X}^*_u$	$\left(\overset{\circ}{X}_{u_w}+\overset{\circ}{X}_{u_p}\right)$	$\overset{\circ}{Y}^*_v$	$\left(\overset{\circ}{Y}_{v_w}+\overset{\circ}{Y}_{v_p}\right)$
$\overset{\circ}{X}^*_w$	$\left(\overset{\circ}{X}_{w_w}+\overset{\circ}{X}_{w_p}\right)$	$\overset{\circ}{Y}^*_p$	$-\left(z_{w_e}\overset{\circ}{Y}_{v_w}+z_{p_e}\overset{\circ}{Y}_{v_p}\right)$
$\overset{\circ}{X}^*_q$	$\left(z_{w_e}\overset{\circ}{X}_{u_w}+z_{p_e}\overset{\circ}{X}_{u_p}-x_{w_e}\overset{\circ}{X}_{w_w}-x_{p_e}\overset{\circ}{X}_{w_p}\right)$	$\overset{\circ}{Y}^*_r$	$\left(x_{w_e}\overset{\circ}{Y}_{v_w}+x_{p_e}\overset{\circ}{Y}_{v_p}\right)$
$\overset{\circ}{Z}^*_u$	$\left(\overset{\circ}{Z}_{u_w}+\overset{\circ}{Z}_{u_p}\right)$	$\overset{\circ}{L}^*_v$	$\left(\overset{\circ}{L}_{v_w}-z_{w_e}\overset{\circ}{Y}_{v_w}-z_{p_e}\overset{\circ}{Y}_{v_p}\right)$
$\overset{\circ}{Z}^*_w$	$\left(\overset{\circ}{Z}_{w_w}+\overset{\circ}{Z}_{w_p}\right)$	$\overset{\circ}{L}^*_p$	$\left(\overset{\circ}{L}_{p_w}-z_{w_e}\left(\overset{\circ}{L}_{v_w}-z_{w_e}\overset{\circ}{Y}_{v_w}\right)+z^2_{p_e}\overset{\circ}{Y}_{v_p}\right)$
$\overset{\circ}{Z}^*_q$	$\left(\overset{\circ}{Z}_{q_w}+z_{w_e}\overset{\circ}{Z}_{u_w}+z_{p_e}\overset{\circ}{Z}_{u_p}-x_{w_e}\overset{\circ}{Z}_{w_w}-x_{p_e}\overset{\circ}{Z}_{w_p}\right)$	$\overset{\circ}{L}^*_r$	$\left(\overset{\circ}{L}_{r_w}+x_{w_e}\left(\overset{\circ}{L}_{v_w}-z_{w_e}\overset{\circ}{Y}_{v_w}\right)-z_{p_e}x_{p_e}\overset{\circ}{Y}_{v_p}\right)$
$\overset{\circ}{M}^*_u$	$\left(\overset{\circ}{M}_{u_w}-x_w\overset{\circ}{Z}_{u_w}+z_w\overset{\circ}{X}_{u_w}-x_p\overset{\circ}{Z}_{u_p}+z_p\overset{\circ}{X}_{u_p}\right)$	$\overset{\circ}{N}^*_v$	$\left(\overset{\circ}{N}_{v_w}+x_{w_e}\overset{\circ}{Y}_{v_w}+x_{p_e}\overset{\circ}{Y}_{v_p}\right)$
$\overset{\circ}{M}^*_w$	$\left(\overset{\circ}{M}_{w_w}-x_w\overset{\circ}{Z}_{w_w}+z_w\overset{\circ}{X}_{w_w}-x_p\overset{\circ}{Z}_{w_p}+z_p\overset{\circ}{X}_{w_p}\right)$	$\overset{\circ}{N}^*_p$	$\left(\overset{\circ}{N}_{p_w}-z_{w_e}\left(\overset{\circ}{N}_{v_w}+x_{w_e}\overset{\circ}{Y}_{v_w}\right)-x_{p_e}z_{p_e}\overset{\circ}{Y}_{v_p}\right)$
$\overset{\circ}{M}^*_q$	$\left(\begin{array}{l}\overset{\circ}{M}_{q_w}+\overset{\circ}{M}_{q_p}+z_w\overset{\circ}{M}_{u_w}-x_w\overset{\circ}{M}_{w_w}-x_w\overset{\circ}{Z}_{q_w}\\ -x_wz_w\overset{\circ}{Z}_{u_w}+x^2_w\overset{\circ}{Z}_{w_w}+z^2_w\overset{\circ}{X}_{u_w}-x_wz_w\overset{\circ}{X}_{w_w}\\ -x_pz_p\overset{\circ}{Z}_{u_p}+x^2_p\overset{\circ}{Z}_{w_p}+z^2_p\overset{\circ}{X}_{u_p}-x_pz_p\overset{\circ}{X}_{w_p}\end{array}\right)$	$\overset{\circ}{N}^*_r$	$\left(\overset{\circ}{N}_{r_w}+\overset{\circ}{N}_{r_p}+x_{w_e}\left(\overset{\circ}{N}_{v_w}+x_{w_e}\overset{\circ}{Y}_{v_w}\right)+x^2_{p_e}\overset{\circ}{Y}_{v_p}\right)$

$$M_e = M_{0_w}+\left(z_{w_e}L_w+x_{w_e}D_w+x_{p_e}D_p\right)\text{Sin}\,\alpha_e$$

$$+\left(x_{w_e}L_w-z_{w_e}D_w-z_{p_e}D_p\right)\text{Cos}\,\alpha_e=0$$

$$N_e=0$$

The longitudinal trim control angle δ_e may be determined from the steady pitching moment M_e in Equation (27).

3.11 The small perturbation equations of motion

For small perturbation motion about trim, the zero expressions given in Equations (27) are substituted into Equations (26) to give the small perturbation equations of motion. Since longitudinal and lateral-directional motion is decoupled the equations of motion may be written, in the state space matrix formulation, for longitudinal motion,

$$\begin{bmatrix}m&0&0&0\\0&m&0&0\\0&0&I_y&0\\0&0&0&1\end{bmatrix}\begin{bmatrix}\dot{u}\\\dot{w}\\\dot{q}\\\dot{\theta}\end{bmatrix}$$

$$=\begin{bmatrix}\overset{\circ}{X}^*_u&\overset{\circ}{X}^*_w&\left(\overset{\circ}{X}^*_q-W_e\right)&-mg\,\text{Cos}\,\theta_e\\ \overset{\circ}{Z}^*_u&\overset{\circ}{Z}^*_w&\left(\overset{\circ}{Z}^*_q+U_e\right)&-mg\,\text{Sin}\,\theta_e\\ \overset{\circ}{M}^*_u&\overset{\circ}{M}^*_w&\overset{\circ}{M}^*_q&0\\0&0&1&0\end{bmatrix}\begin{bmatrix}u\\w\\q\\\theta\end{bmatrix}+\begin{bmatrix}0\\0\\\overset{\circ}{M}^*_\delta\\0\end{bmatrix}\delta \quad \ldots(28)$$

and for lateral-directional motion,

$$\begin{bmatrix}m&0&0&0&0\\0&I_x&-I_{xz}&0&0\\0&-I_{xz}&I_z&0&0\\0&0&0&1&0\\0&0&0&0&1\end{bmatrix}\begin{bmatrix}\dot{v}\\\dot{p}\\\dot{r}\\\dot{\phi}\\\dot{\psi}\end{bmatrix} \quad \ldots(29)$$

Table 2
Equivalent aerodynamic control derivatives
Referred to body axes

$\overset{\circ}{M}^*_\delta$	$\frac{m_pl_2}{m}\text{Cos}\delta_e\left(L_w\text{Cos}\left(\delta_e-\alpha_e\right)+\left(D_w-\frac{m_w}{m_p}D_p\right)\text{Sin}\left(\delta_e-\alpha_e\right)\right)$
$\overset{\circ}{L}^*_\xi$	$\frac{m_pl_2}{m}L_w\text{Cos}\delta_e\text{Cos}\alpha_e$
$\overset{\circ}{N}^*_\xi$	0

$$= \begin{bmatrix} \overset{\circ}{Y}^*_v & \left(\overset{\circ}{Y}^*_p + W_e\right) & \left(\overset{\circ}{Y}^*_r - U_e\right) & mg\,\mathrm{Cos}\,\theta_e & mg\,\mathrm{Sin}\,\theta_e \\ \overset{\circ}{L}^*_v & \overset{\circ}{L}^*_p & \overset{\circ}{L}^*_r & 0 & 0 \\ \overset{\circ}{N}^*_v & \overset{\circ}{N}^*_p & \overset{\circ}{N}^*_r & 0 & 0 \\ 0 & 1 & 0 & 0 & 0 \\ 0 & 0 & 1 & 0 & 0 \end{bmatrix} \begin{bmatrix} v \\ p \\ r \\ \phi \\ \psi \end{bmatrix} + \begin{bmatrix} 0 \\ \overset{\circ}{L}^*_\xi \\ \overset{\circ}{N}^*_\xi \\ 0 \\ 0 \end{bmatrix} \xi$$

4.0 AERODYNAMIC MODEL

Original full scale experimental research by Kilkenny[1] and Sweeting[14] provided longitudinal lift, drag and pitching moment data for a number of hang glider wings. Further, Kilkenny[4] also carried out full scale wind tunnel experiments on hang glider pilots in the natural flying attitude which produced similar aerodynamic data. The most comprehensive set of aerodynamic data was obtained for the Hiway 'Demon' hang glider wing, and this data has been used as the basis for the present application.

It is notable that the aerodynamic properties of the hang glider wing are significantly non-linear. Since the wing is flexible its shape adjusts to the loading condition subject to the physical constraints imposed by the rigid structure. In simple terms it is evident that the non-linearity arises from variations in camber and span-wise twist due to velocity and angle-of-attack variation over the operating flight envelope. A research study undertaken by Powton[7] resulted in the development of mathematical expressions for lift, drag and pitching moment as analytical functions of camber and twist. The aerodynamic model developed for the present application is derived from those original expressions. This approach to aerodynamic modelling was chosen since it represents a working compromise between simplicity and accuracy; it replicates the main features of hang glider aerodynamic behaviour whilst retaining a high level of visibility of the underlying physical phenomena driving the aerodynamic behaviour. Further, the original experimental data set provided the means to calibrate and validate the aerodynamic model.

The approach taken by Powton[7] was semi-empirical in which the applicable physical phenomena were assumed to have a particular dependence on air speed or incidence, or both. The constants in the mathematical expressions were then determined from the experimental longitudinal data. This ensures that the fundamental influences on the aerodynamic behaviour can be identified easily. However, a significant limitation of the aerodynamic model derived from this source material is that it is inherently quasi-static. Thus, although trim aerodynamic conditions can, with minimal experimental data, be estimated with reasonable accuracy, unsteady aerodynamic and apparent mass effects are not accounted for.

4.1 Wing luffing

Luffing is a phenomenon uniquely associated with flexible wings (sails) and occurs when the local angle-of-attack falls below a certain value, dependent on velocity, and, typically, this occurs over an inboard fraction of the semi-span only. Lower angles of attack are associated with higher glide velocities implying higher aerodynamic wing loading. In response to the increased aerodynamic load the flexible wing camber and spanwise twist can change significantly. In normal flight at higher positive angles of attack the wing is fully inflated and maintains a highly cambered aerofoil like shape which is constrained to an extent by pre-formed chord-wise stiffening battens. However, as the angle-of-attack is reduced the degree of inflation diminishes in combination with increasing spanwise washout and at the luffing angle-of-attack α_L the wing starts to deflate from the trailing edge with a corresponding change in its aerodynamic properties. The result is a trailing edge down camber change which can result in an abrupt and potentially dangerous nose down pitching moment. Typically, luffing occurs at angles of attack below approximately 5°. To protect the glider against uncontrolled departure into a luffing dive, luff lines are fitted to introduce stabilising reflex camber into the wing at angles of attack below the luffing angle-of-attack.

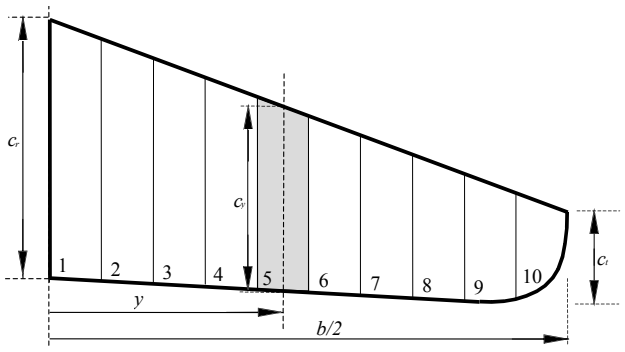

Figure 8. Wing panel segment model.

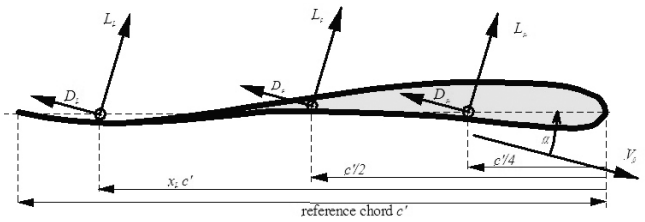

Figure 9. Aerofoil lift and drag distribution.

4.2 Aerodynamic model development

Powton[7] decided that the most easily interpreted approach to modelling the aerodynamics of the hang-glider wing was to divide the semi-span into ten chord-wise segments, as indicated on Fig. 8.

The wing twist across the semi-span then defines the angle-of-attack of each segment which is treated as a 2D aerofoil. By predicting general forms for various airfoil section characteristics as functions of angle-of-attack α and velocity V, and assuming these to be constant for each segment, the sum of the segment characteristics across the span determines an estimate of the aerodynamic characteristics of the wing. This approach was adopted in preference to integral calculus because the functions describing the section aerodynamics are not necessarily continuous across the semi-span. Preliminary studies showed that dividing the semi-span into more than ten segments of equal width did not greatly improve the accuracy of the model but did significantly increase the computational effort required.

The main physical phenomena which determine the aerodynamic properties of the wing are the variation of span-wise twist with incidence and velocity, and the variation of section lift coefficient due to incidence, camber and action of the luff lines. Wing twist is a significant contributor to aerodynamic non-linearity and Nickel and Wolhfahrt[15] describe it as a common feature of hang gliders operating at normal flight conditions. Wing twist angles in excess of 45° at stall angles of attack were observed experimentally by Kilkenny[1]. Typical hang glider wings are fitted with fixed rigid chord-wise 'tip rods' which limit the trailing edge down wing tip twist angle to a preset value.

Referring to Fig. 9, the aerodynamic force due to a wing section may be separated into three components, lift due to incidence, lift due to camber and lift due to the action of the luff lines.

As for the standard rigid airfoil, lift due to incidence L_α acts at the quarter-chord point and the lift due to camber L_c acts at the mid-chord point. However, the lift due to camber is not constant because the hang glider airfoil is flexible and changes shape with loading. The lift due to the action of the luff lines L_L is assumed to act at a constant fraction x_L of the section chord measured from the leading edge. It is clear that, even in the absence of luff lines, the pitching moment of the hang glider aerofoil section about the quarter-chord point is not constant with incidence because the lift due to camber varies due to the flexible nature of the aerofoil. Thus, the concept of a nominally constant aerodynamic centre position for all flight conditions is not appropriate for the hang glider. Cook[6] has previously defined an alternative approach in which all pitching moments are referenced to a fixed aerodynamic reference point *arp* which, in this work, is located on the keel coincident with the apex of the control frame.

4.3 Wing twist

Powton[7] devised a wing twist model based on the assumption that the maximum twist at the wing tip ε_T relative to the centre line chord is an exponential function of velocity and a linear function of the wing area normal to the free stream. Thus the function is of the general form,

$$\varepsilon_T = k_1 \text{ Sin } \alpha_R + k_2 e^{k_3 V} \quad \ldots (30)$$

where k_1, k_2 and k_3 are constants determined empirically from experimental data. Further, the experimental evidence suggests that span-wise twist distribution is non-linear since the torsional stiffness of the wing reduces towards the tip. A quadratic function of the following general form was assumed to describe the local twist ε_y at span-wise co-ordinate y,

$$\varepsilon_y = 4\varepsilon_T \left(\frac{y}{b}\right)^2 \quad \ldots (31)$$

4.4 Lift due to incidence

It is assumed that the lift due to incidence of the hang-glider airfoil section is proportional to the angle-of-attack when it is greater than the luffing angle-of-attack α_L. For angles of attack below the luffing angle-of-attack the lift due to incidence is assumed to be a function of the square of the speed. Further, the incidence at which luffing commences increases with increasing velocity. Once luffing has commenced, the lift generated by the wing section decreases and, for simplicity, it is assumed that at incidences below α_L the lift generated by the section for a given incidence remains constant. Accordingly, general expressions for the lift coefficient due to incidence may be written,

$$\begin{aligned} C_{L_\alpha} &= a_1\alpha && \text{for } \alpha > \alpha_L \\ C_{L_\alpha} &= a_1\alpha_L = a_1\left(k_4V^2 + k_5\right) && \text{for } \alpha \le \alpha_L \end{aligned} \quad \ldots (32)$$

where a_1 is the lift curve slope and k_4 and k_5 are constants determined empirically from experimental data.

4.5 Lift due to camber

It is hypothesised that the lift generated by a flexible wing comprises two contributions, lift due to incidence as for a rigid wing, plus lift due to an increase in camber. As incidence is increased the pressure distribution around the wing causes the shape of the flexible wing to adapt to minimise loading and the result is an increase in camber. A velocity dependency is also evident since an increase in velocity increases the pressure distribution around the flexible wing resulting in an increase in camber. However, increasing camber presents a greater cross section area to the free stream. Consequently, energy considerations suggest that the camber of the wing is likely to be only weakly dependent on velocity since it will adapt to minimise loading by reducing camber.

Since the wing has positive camber when it is unloaded due to the way it is rigged and to the pre-formed chord wise stiffening battens, it is assumed that the rate of change of camber with incidence is greater for positive incidence. Accordingly, Powton[7] proposed the following general form for lift coefficient due to camber,

$$\begin{aligned} C_{L_c} &= \frac{a_{21}\alpha + k_6}{V^2} && \text{for } \alpha \ge 0 \\ C_{L_c} &= \frac{a_{22}\alpha + k_6}{V^2} && \text{for } \alpha < 0 \end{aligned} \quad \ldots (33)$$

where, a_{21} and a_{22} are the effective lift curve slopes accounting for changes in incidence due to camber and k_6 is a constant, all of which are determined empirically from experimental data.

4.6 Lift due to the action of luff lines

For all angles-of-attack below a pre-set value, the luff lines become taut and prevent any further trailing-edge camber developing. Consequently the wing section adopts a reflex camber shape towards the trailing edge which introduces a negative lift increment together with a nose up pitching moment. This is most conveniently modelled by assuming the point of action is located at $x_L c'$ as indicated in Fig. 9.

The reasoned approach made by Powton[7] was similar to his consideration of camber effects in which it is assumed that lift coefficient due to the action of the luff lines C_{L_L} is proportional to incidence and inversely proportional to the square of velocity. The section trailing edge shape is thus effectively independent of velocity and this correlates with experimental observation that the luff lines become taut at a fixed root chord incidence independent of velocity. If the root incidence at which the luff lines become tight is denoted α_{R_L} and the root incidence at which the reflex reaches a maximum is denoted α'_{R_L}, then the lift coefficient due to the action of the luff lines may be written,

$$\begin{aligned} C_{L_L} &= 0 && \text{for } \alpha_R \ge \alpha_{R_L} \\ &\text{(luff lines slack)} \\ C_{L_L} &= \frac{a_3\left(\alpha_R - \alpha_{R_L}\right)}{V^2} && \text{for } \alpha'_{R_L} < \alpha_R < \alpha_{R_L} \\ &\text{(luff lines tightening)} \\ C_{L_L} &= \frac{a_3\left(\alpha'_{R_L} - \alpha_{R_L}\right)}{V^2} && \text{for } \alpha_R \le \alpha'_{R_L} \\ &\text{(luff lines taut)} \end{aligned} \quad \ldots (34)$$

where a_3 is the equivalent lift curve slope due to the action of the luff lines and is determined from experimental data.

5.0 AERODYNAMIC MODEL DATA

Measured aerodynamic data for the Hiway Demon hang glider wing was used as the basis for the application of the mathematical modelling described above. Original experiments by Kilkenny[1] produced aerodynamic data at a number of test speeds representative of the flight envelope of the hang glider. For the convenience of data

Table 3
Hiway Demon configuration

Pilot mass	m_p	80kg
Wing mass	m_w	31kg
Total mass	m	111kg
Wing area	S	16·26m^2
Wing span	b	10m
Reference chord length	c'	1.626m
LE of c' from nose		1·26m
Dihedral angle	Γ	1deg
Hang strap length	l_2	1·2m
arp position on c'		0·215
Hang point position on c'		0·246
Control frame attachment on c'		0·185
Pilot drag coefficient	C_{Dp}	0·009
Control frame drag coefficient	C_{Df}	0·007

comparison, mathematically modelled aerodynamic parameters were evaluated at the same velocity values. The principal parameters describing the configuration of the hang glider as used in the present analysis are set out in Table 3. Note that the only contributions of the pilot and control frame to the aerodynamics of the hang glider are drag, and that both coefficients are nominally constant. The drag coefficients given in Table 3 are referenced to wing area.

Using the lift model defined by Equations (30) to (34), Powton[7] estimated the lift, drag and pitching moment characteristics of each segment and hence, by simple summation, the total for the entire wing. Comparison with measured experimental data for the Hiway Demon wing indicated that the lift and drag estimates were generally in good agreement, but that the pitching moment estimate was poor. The reasons for this poor match were not resolved, but it is known that the original experimental pitching moment data is of limited integrity, especially at lower speeds.

Spottiswoode[9] used Powton's aerodynamic model as the basis for the flight dynamics modelling. However, small adjustments to the empirical constants were made in an attempt to improve the fidelity, especially of the pitching moment. Lift, drag and pitching moment coefficients were estimated at a number of speed points over the flight envelope. Comparisons of the estimated coefficients were made with coefficients derived directly from the original smoothed experimental data as shown on Fig. 10, Fig. 11 and Fig. 12 respectively. In each case data comparisons are made for two speeds,

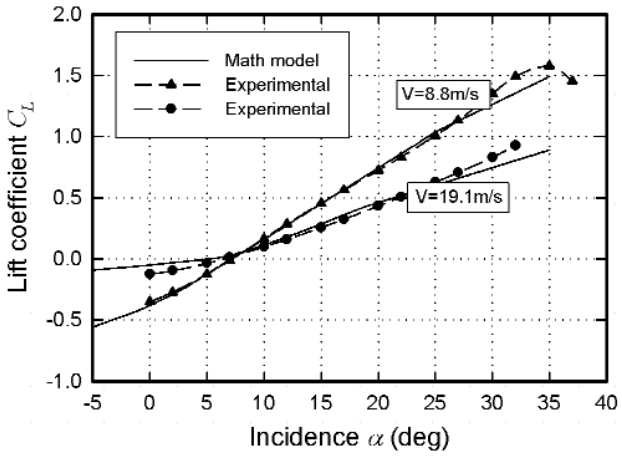

Figure 10. Lift coefficient comparison.

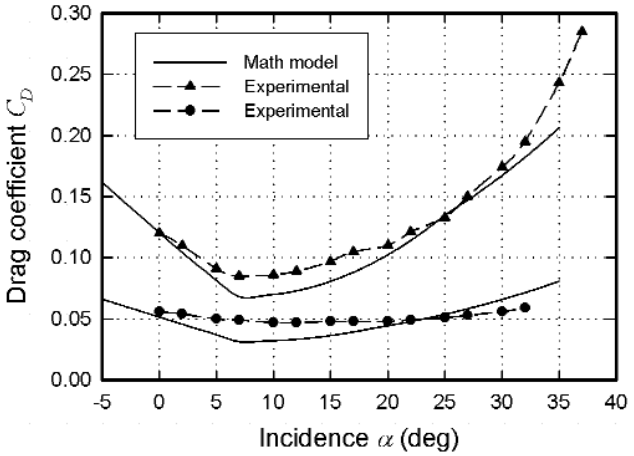

Figure 11. Drag coefficient comparison.

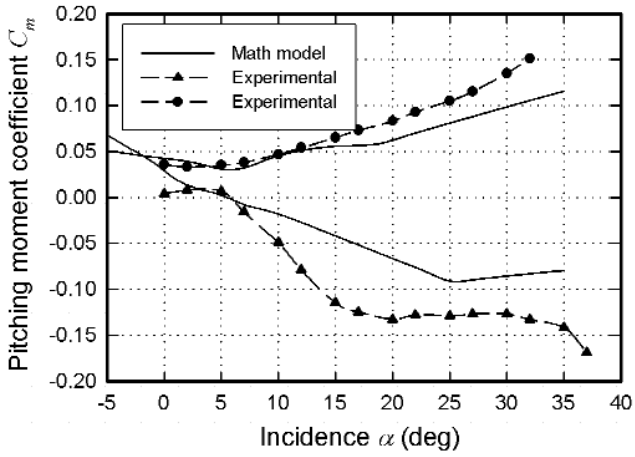

Figure 12. Pitching moment coefficient comparison.

8·8ms^{-1} and 19·1ms^{-1}, being the minimum and maximum speeds tested in the original experimental programme.

The mathematical model can be seen to provide a good approximation to the experimental lift and drag values and an adequate approximation to the experimental moment coefficient values. The most notable non-linear behaviour is that of the moment coefficient, particularly the strong negative moment at low airspeeds. This occurs since the lift coefficient due to aerofoil camber is inversely proportional to the square of the airspeed, while the lift coefficient due to incidence is independent of airspeed. The net effect at low speeds is that the lift due to camber dominates, therefore causing a rearwards shift of the centre of pressure and hence a nose down pitching moment. Other aspects of the aerodynamic behaviour are comprehensively described by Powton[7].

6.0 AERODYNAMIC TRIM

In order to apply the linearised equations of motion, it is first necessary to determine the aerodynamic operating point. Accordingly, the longitudinal aerodynamic trim condition was calculated using the procedure described by Cook[6]. The trim condition was estimated for each of the speeds for which comparative experimental data was

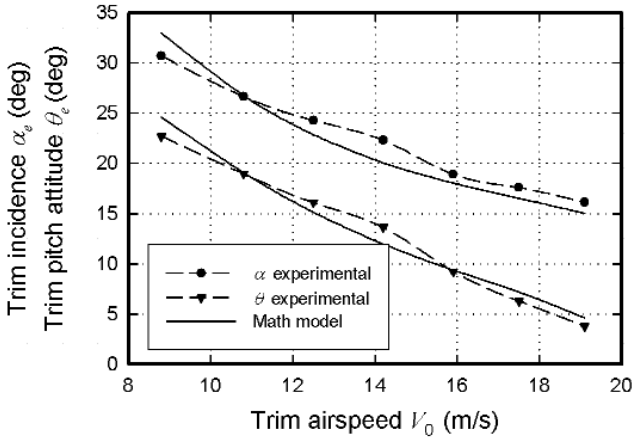

Figure 13. Trim incidence and pitch attitude comparisons.

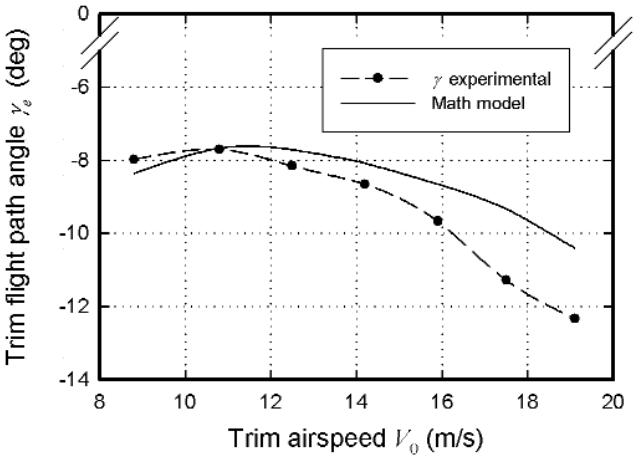

Figure 14. Trim flight path angle comparison.

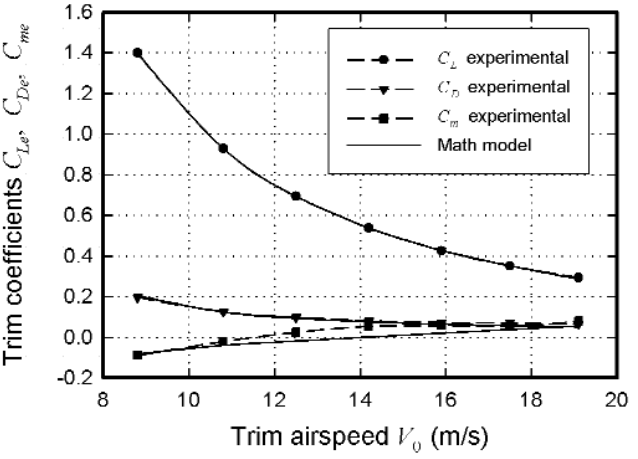

Figure 15. Trim lift, drag and pitching moment coefficients comparison.

available. In the interests of simplicity the pilot mass, hang point position and hang strap length were given typical values as defined in Table 3.

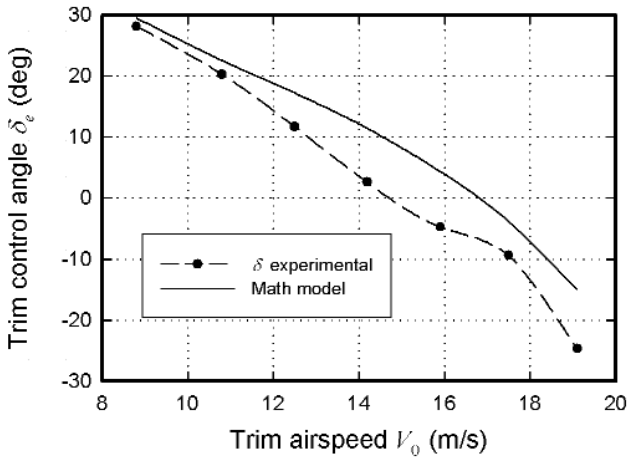

Figure 16. Trim longitudinal control angle comparison.

Solution of the trim equations yields the trim aerodynamic coefficients, pitch attitude, flight path angle and longitudinal control angle for each flight case. The values obtained using experimental aerodynamic data and the values estimated by the mathematical model are plotted in Fig. 13 to Fig. 16. It is evident that values estimated by the mathematical model correlate well with those obtained from the experimental data. In particular, the modelled trim coefficients shown on Fig. 15 correlate extremely well with the experimental values. The trim conditions thus derived are also in good agreement with the values obtained by Cook[6], which provides validation of the implementation and gives confidence in the mathematical modelling.

The data plotted in Fig. 13 and Fig. 16 suggest a reasonably linear trend of pitch attitude and angle-of-attack as a function of trim longitudinal control angle. This implies well behaved longitudinal trim characteristics; i.e. the pilot would see a predictable change in trim condition for a given input.

Now the trim pitching moment coefficient shown in Fig. 15 suggests that it is adequately modelled and that it is almost linear. Thus the difference between the experimental and model trim control angles as shown in Fig. 16 suggest a strong dependency on the accuracy of the aerodynamic model used in the estimation procedure. Given the difficulty of determining a representative pitching moment model compatible with the experimental observations, this is not entirely surprising. However, it is considered that the fidelity of the model is good enough for present purposes.

Trim flight path angle is shown on Fig. 14 from which it may be determined that the best glide angle corresponds approximately with an airspeed of 11ms^{-1}, the minimum drag speed. The best glide angle is approximately 7·5°, which compares well with the value of 7·4° reported by Kilkenny[1].

7.0 AERODYNAMIC STABILITY AND CONTROL DERIVATIVES

The aerodynamic stability derivative contributions were estimated for the wing, the pilot and the control frame, and summed to give the total derivative values for the hang glider. The computation was repeated for each of the seven trimmed speed points embracing the flight envelope. The computational procedures adopted by Spottiswoode[9] included application of the simple derivative models such as those given in Cook[13], the use of ESDU[16] estimates and first principles where no other method was appropriate. In appropriate cases, the aerodynamic derivatives for the wing were

Table 4
Equivalent longitudinal dimensionless stability derivatives. Referred to wind axes

V_0 ms^{-1}	X_u^*	Z_u^*	X_w^*	Z_w^*	M_u^*	M_w^*	X_q^*	Z_q^*	M_q^*
8·8	–0·258	–2·364	0·944	–2·811	0·182	–0·483	0·1321	0·189	–0·643
10·8	–0·179	–1·466	0·675	–2·326	0·172	–0·281	0·0881	–0·040	–0·555
12·5	–0·136	–1·189	0·511	–2·209	0·121	–0·238	0·0677	–0·142	–0·541
14·2	–0·110	–0·987	0·376	–2·482	0·084	–0·393	0·0591	–0·397	–0·690
15·9	–0·093	–0·837	0·314	–2·291	0·053	–0·410	0·0598	–0·504	–0·701
17·5	–0·081	–0·747	0·260	–2·209	0·021	–0·474	0·0623	–0·651	–0·725
19·1	–0·085	–0·696	0·210	–2·151	–0·005	–0·578	0·0708	–0·842	–0·761

Table 5
Equivalent lateral–directional dimensionless stability derivatives. Referred to wind axes

V_0 ms^{-1}	Y_v^*	L_v^*	N_v^*	Y_p^*	L_p^*	N_p^*	Y_r^*	L_r^*	N_r^*
8·8	–0·226	–0·465	0·0378	–0·0164	–0·5837	0·0367	0	0·2411	–0·0489
10·8	–0·226	–0·322	0·0275	–0·0163	–0·4694	0·0284	0·0002	0·1632	–0·0289
12·5	–0·226	–0·249	0·0177	–0·0162	–0·4131	0·0223	0·0007	0·1232	–0·0211
14·2	–0·226	–0·196	0·0124	–0·0161	–0·3760	0·0179	0·0016	0·0930	–0·0167
15·9	–0·226	–0·157	0·0107	–0·0157	–0·3488	0·0150	0·0030	0·0690	–0·0140
17·5	–0·226	–0·129	0·0111	–0·0151	–0·3237	0·0129	0·0049	0·0531	–0·0123
19·1	–0·226	–0·104	0·0129	–0·0139	–0·2702	0·0107	0·0075	0·0411	–0·0112

estimated for each of the chordwise segments and summed to give the total value. Due to the complexity and discontinuous nature of many of the functions involved, the derivatives were obtained numerically using Mathcad computational tools. The generic approach comprised interpolation between the discrete data points generated by the aerodynamic model using cubic splines, and numerically differentiating the resulting function to obtain the gradient of the curve at the desired test point. A listing of the substantial Mathcad program is given in Spottiswoode[9].

The aerodynamic stability derivatives were estimated in accordance with the descriptions given in Table 1 in order to have direct compatibility with the equations of motion set out in Equations (28) and (29). However, for analytical convenience they were transformed to a wind axes reference with origin coincident with the *cg*. It should be remembered that the *cg* position varies with trim condition since it is the principal control variable. Dimensionless values of the equivalent derivatives thus obtained are set out in Tables 4 and 5.

Familiar derivatives not appearing in Tables (4) and (5) were found to be insignificantly small and consequently omitted.

Similarly, estimates of the equivalent dimensionless aerodynamic control derivatives were made in accordance with the expressions given in Table (2). Dimensionless values of the equivalent control derivatives thus obtained are set out in Table (6).

Table 6
Equivalent dimensionless control derivatives
Referred to wind axes

V_0 ms^{-1}	M_δ^*	L_ξ^*
8·8	0·6092	0·1052
10·8	0·4416	0·0742
12·5	0·3478	0·0573
14·2	0·2803	0·0455
15·9	0·2282	0·0369
17·5	0·1852	0·0304
19·1	0·1376	0·0239

Table 7
Moments and product of inertia. Referred to wind axes

V_0 ms^{-1}	I_x kgm^2	I_y kgm^2	I_z kgm^2	I_{xz} kgm^2
8·8	249·86	112·11	248·60	–35·20
10·8	242·17	111·81	255·99	–30·54
12·5	237·77	111·58	260·16	–26·30
14·2	234·60	111·32	263·06	–21·84
15·9	231·73	110·99	265·61	–17·01
17·5	228·37	110·61	268·59	–12·14
19·1	223·02	110·09	273·42	–6·82

8.0 MOMENTS OF INERTIA

Since *cg* shifting is the primary mechanism for control of the hang glider, the moments and product of inertia referenced to axes originating at the *cg* vary with each trimmed flight condition. Total inertia values represent the sum of the wing inertias and the inertias of the pilot. As indicated earlier, the pilot is represented by a cylindrical body having a uniform mass distribution and with its axis of symmetry parallel to the keel datum axis of the wing. The hang strap is attached to the pilot at the *cg* of the cylinder. Calculation of inertias then becomes a simple application of the parallel axis theorem. The moments and product of inertia values calculated for each trim speed and transformed to a wind axes reference are set out in Table 7.

9.0 THE LINEAR FLIGHT DYNAMICS OF THE HANG GLIDER

Since the flight envelope speed range of the hang glider is very small, the observable changes in its flight dynamics characteristics are correspondingly modest. Although changes in characteristics due to wing flexibility are discernible, they are quite predictable. Consequently the following analysis is limited to one trimmed flight condition only. The case chosen is representative of the optimum glide condition at a speed of 10·8ms^{-1}, and is typical of the speed a pilot would choose to maximise his flight time. Thus a pilot would choose to operate at, or near this speed except when manoeuvring. A

complete analysis for the speed envelope may be found in Spottiswoode[9].

9.1 Longitudinal equations of motion

The longitudinal dimensional stability and control derivatives were calculated in the usual way from the values given in Tables 4 and 6, and together with the mass and corresponding inertia values from Table 7 were substituted into the longitudinal equations of motion (28) – noting that a wind axes reference applies. Dividing through by the mass matrix results in the longitudinal state equation,

$$\begin{bmatrix}\dot{u}\\ \dot{w}\\ \dot{q}\\ \dot{\theta}\end{bmatrix}=\begin{bmatrix}-0.1730 & 0.6538 & 0.1388 & -9.7222\\ -1.4208 & -2.2535 & 10.7370 & 1.3093\\ 0.2685 & -0.4402 & -1.4113 & 0\\ 0 & 0 & 1 & 0\end{bmatrix}\begin{bmatrix}u\\ w\\ q\\ \theta\end{bmatrix}+\begin{bmatrix}0\\ 0\\ 7.46\\ 0\end{bmatrix}\delta \quad \ldots (35)$$

9.2 Longitudinal response transfer functions

Solution of the longitudinal state Equation (35) yields the response transfer functions,

$$\begin{aligned}\frac{u(s)}{\delta(s)}&=\frac{1.036(s+6{\cdot}417)(s-23{\cdot}63)}{(s^2-0{\cdot}18s+1{\cdot}34)(s^2+4{\cdot}02s+8{\cdot}8)} \quad \frac{\text{m/s}}{\text{rad}}\\ \frac{w(s)}{\delta(s)}&=\frac{80{\cdot}1(s^2+0{\cdot}277s+1{\cdot}306)}{(s^2-0{\cdot}18s+1{\cdot}34)(s^2+4{\cdot}02s+8{\cdot}8)} \quad \frac{\text{m/s}}{\text{rad}}\\ \frac{q(s)}{\delta(s)}&=\frac{7{\cdot}46s(s+0{\cdot}822)(s+1{\cdot}605)}{(s^2-0{\cdot}18s+1{\cdot}34)(s^2+4{\cdot}02s+8{\cdot}8)} \quad \frac{1}{\text{s}}\\ \frac{\theta(s)}{\delta(s)}&=\frac{7{\cdot}46(s+0{\cdot}822)(s+1{\cdot}605)}{(s^2-0{\cdot}18s+1{\cdot}34)(s^2+4{\cdot}02s+8{\cdot}8)}\end{aligned} \quad \ldots (36)$$

9.3 Longitudinal stability modes

With reference to Equations (36) the classical longitudinal characteristic equation is given by,

$$\Delta(s)=(s^2-0{\cdot}18s+1{\cdot}34)(s^2+4{\cdot}02s+8{\cdot}8)=0 \quad \ldots (37)$$

The first pair of complex roots describes the unstable phugoid mode with damping ζ_{ph} = –0·078 and frequency ω_{ph} = 1·16 rad/s. The second pair of complex roots describes the classical short period pitching mode with damping ζ_{sp} = 0·68 and frequency ω_{sp} = 2·97 rad/s.

To give an indication in the variation of the longitudinal stability of the hang glider over its speed envelope, the phugoid mode and short period pitching mode characteristics are plotted in Fig. 17 and Fig. 18 respectively. The frequency and damping ratio of the phugoid mode are consistent with the understanding of basic flight physics. However, the main departures from the norm, namely higher than usual frequency and large damping ratio magnitude at extreme speeds are due to significant positive derivative M_u. At low speed, pitching moment is usually independent of speed and hence the derivative is insignificant. However, this is not the case with the

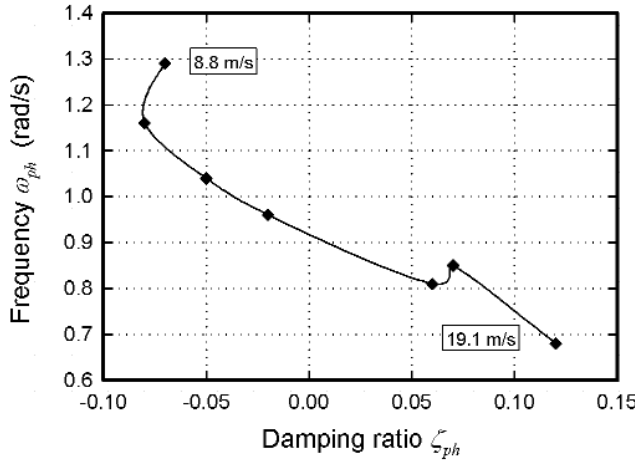

Figure 17. Phugoid mode characteristic.

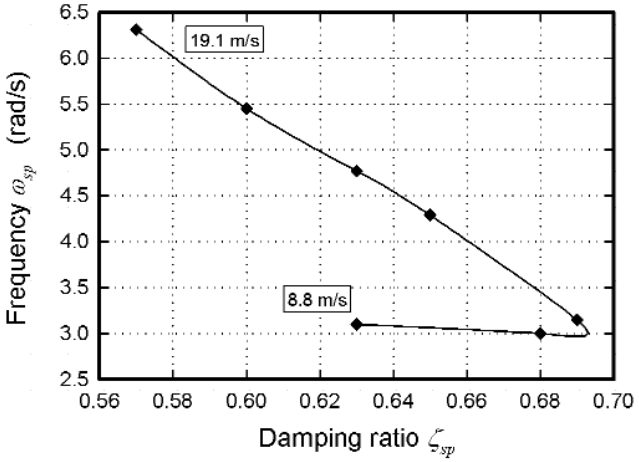

Figure 18. Short period pitching mode characteristic.

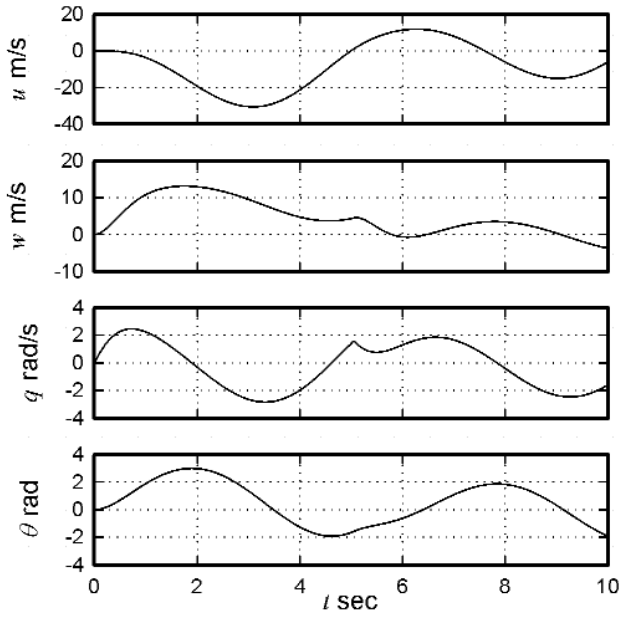

Figure 19. Longitudinal response to 1 rad/5s square pulse input.

hang glider since the pitching moment is significantly dependent on wing shape which is very dependent on speed. In Fig. 17 the inconsistency at 17·5ms^{-1} is thought to be due to the poor quality pitching moment data on which the empirical models are based.

The short period pitching mode characteristic shown on Fig. 18 is entirely consistent with conventional theory. The inflexion in damping at lower speed is due to the way in which the estimate for M_q varies with speed. This may be due to the fact that the speed at this point is close to the minimum drag speed, or it may be due to the poor quality pitching moment data on which the model is based.

9.4 Typical longitudinal response dynamics

The time response to a square pulse input representing a steady push by the pilot for five seconds is shown on Fig. 19. Since input causes a nose up response the hang glider slows down and this is clearly visible. As the short period mode is highly damped it is not visible as it is masked by the mildly unstable phugoid oscillation. The phugoid is also more evident since its frequency, relative to the short period mode frequency, is rather higher than for a conventional aeroplane.

Since the response plots are divergent, it is difficult to estimate values for the longitudinal static control sensitivity of the hang glider. However, applying the final value theorem to the transfer functions, Equations (36), assuming a unit step control input, then the static control gains are,

$$\begin{aligned} u_{ss} &= -15\cdot47\delta \ \text{m/s/rad} \\ w_{ss} &= 10\cdot3\delta \ \text{m/s/rad or equivalently } \alpha_{ss} = 0\cdot96\delta \\ \theta_{ss} &= 0\cdot97\delta \end{aligned} \qquad \ldots (38)$$

This is entirely consistent with the flight mechanics model of the hang glider which suggests a 1:1 relationship between control angle δ, incidence α and pitch θ.

9.5 Lateral-directional equations of motion

Similarly, the lateral-directional dimensional stability and control derivatives were calculated from the values given in Tables 5 and 6, and together with the mass and corresponding inertia values from Table 7 were substituted into the equations of motion (29) – again noting that a wind axes reference applies. Dividing through by the mass matrix results in the lateral-directional state equation,

$$\begin{bmatrix} \dot{v} \\ \dot{p} \\ \dot{r} \\ \dot{\phi} \\ \dot{\psi} \end{bmatrix} = \begin{bmatrix} -0\cdot2195 & -0\cdot1580 & -10\cdot798 & 9\cdot722 & -1\cdot3098 \\ -1\cdot4670 & -21\cdot318 & 7\cdot5163 & 0 & 0 \\ 0\cdot2906 & 3\cdot7362 & -2\cdot1119 & 0 & 0 \\ 0 & 1 & 0 & 0 & 0 \\ 0 & 0 & 1 & 0 & 0 \end{bmatrix} \begin{bmatrix} v \\ p \\ r \\ \phi \\ \psi \end{bmatrix} + \begin{bmatrix} 0 \\ 3\cdot6136 \\ -0\cdot4311 \\ 0 \\ 0 \end{bmatrix} \xi \qquad \ldots (39)$$

9.6 Lateral-directional response transfer functions

Solution of the lateral-directional state Equation (39) yields the response transfer functions,

$$\begin{aligned} \frac{v(s)}{\xi(s)} &= \frac{4\cdot084s\left(s^2-2\cdot83s+9\cdot072\right)}{s\left(s+0\cdot512\right)\left(s+22\cdot59\right)\left(s^2+0\cdot544s+0\cdot85\right)} \quad \frac{\text{ms}^{-1}}{\text{rad}} \\ \frac{p(s)}{\xi(s)} &= \frac{3\cdot614s\left(s+0\cdot111\right)\left(s^2+1\cdot324s+1\cdot37\right)}{s\left(s+0\cdot512\right)\left(s+22\cdot59\right)\left(s^2+0\cdot544s+0\cdot85\right)} \quad \frac{1}{\text{s}} \\ \frac{r(s)}{\xi(s)} &= \frac{-0\cdot4311s\left(s-10\cdot08\right)\left(s^2+0\cdot295s+0\cdot935\right)}{s\left(s+0\cdot512\right)\left(s+22\cdot59\right)\left(s^2+0\cdot544s+0\cdot85\right)} \quad \frac{1}{\text{s}} \\ \frac{\phi(s)}{\xi(s)} &= \frac{3\cdot614\left(s+0\cdot111\right)\left(s^2+1\cdot324s+1\cdot37\right)}{s\left(s+0\cdot512\right)\left(s+22\cdot59\right)\left(s^2+0\cdot544s+0\cdot85\right)} \\ \frac{\psi(s)}{\xi(s)} &= \frac{-0\cdot4311\left(s-10\cdot08\right)\left(s^2+0\cdot295s+0\cdot935\right)}{s\left(s+0\cdot512\right)\left(s+22\cdot59\right)\left(s^2+0\cdot544s+0\cdot85\right)} \end{aligned} \qquad \ldots (40)$$

9.7 Lateral-directional stability modes

With reference to Equations (40) the lateral-directional characteristic equation is given by,

$$\Delta(s) = s\left(s+0\cdot512\right)\left(s+22\cdot59\right)\left(s^2+0\cdot544s+0\cdot85\right) = 0 \qquad \ldots (41)$$

The zero root in Equation (41) describes the heading integration. The first real root describes the stable spiral mode with time constant T_s = 1·95s. The second real root describes the stable, and very fast, roll mode with time constant T_r = 0·044s. The pair of complex roots describes the classical Dutch roll mode with damping ζ_{dr} = 0·3 and frequency ω_{dr} = 0·92 rad/s. The most striking immediate observation is that all three lateral-directional modes are rather more stable than for a conventional aeroplane.

The roll subsidence mode shows little variation with airspeed, the time constant remaining within the range 0·04s ≤ T_r ≤ 0·05s. The small value obtained for the roll subsidence mode time constant is a direct result of the large value of the derivative L_p. Spottiswoode[9] suggests that the modelling method leads to a probable over estimate of the roll damping derivative since some of the non-linear effects of wing flexibility are not adequately accounted for. However, the roll mode characteristic is plausible if not accurate.

The Dutch roll mode stability characteristic is shown on Fig. 20 and indicates a well damped oscillation with appropriate frequency range. Interpretation of the dynamics focuses on the higher than conventional damping ratio. Spottiswoode[9] undertook eigenvector analysis of the mode which clearly indicates the dominant motion to be sideslip which couples strongly into the highly damped roll with a relatively small yaw component. This is also borne out clearly in the time response shown in Fig. 22. It would seem that the mode is fundamentally a lateral pendulum motion dominated by the suspended mass of the pilot and the high natural damping in roll.

The spiral mode stability characteristic is shown on Fig. 21 and indicates an exceptionally high level of stability with a very short time constant. Again, eigenvector analysis shows the dominant motion to be sideslip which couples strongly into yaw, with very little roll motion. These dominant spiral mode characteristics are also clearly visible in the time response shown in Fig. 22. This strong stability is partly due to the stabilising effect of wing sweep and the absence of a fin helps in this respect. However, the lateral pendulum effect of the suspended pilot mass will also play a part by resisting any tendency to departure in roll. Thus a good degree of natural aerodynamic spiral mode stability is enhanced by the suspended pilot mass.

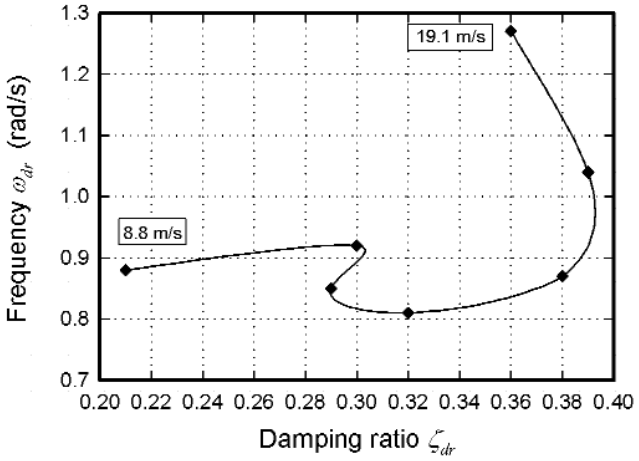

Figure 20. Dutch roll mode characteristic.

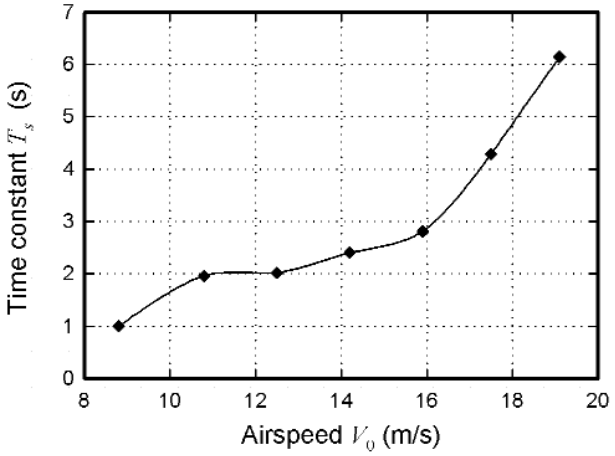

Figure 21. Spiral mode characteristic.

9.8 Typical lateral – directional response dynamics

The time response to a square pulse input representing a steady right lateral displacement (positive) by the pilot for 15 seconds is shown on Fig. 22. Since the control input demands a turn to the right, the hang glider rolls, yaws and sideslips to the right, but it takes five seconds for the turn to become established. This is due to the relatively high level of inherent stability and the relatively weak control effectiveness. The stability modes are clearly visible in the response plots. The very short roll mode time constant is indicated by the instantaneous rise in roll rate *p* when the input is applied and removed. The well damped dutch roll mode is clearly visible in sideslip *v* and roll rate *p* responses. The very stable spiral mode, with two second time constant, is most clearly visible in the slow rise in yaw rate *r* response following the control input. The adverse control effects are not visible, since they are not adequately modelled by the linear equations of motion.

Since the hang glider is stable it is easy to estimate values for the lateral-directional static control sensitivity of the hang glider from inspection of Fig. 22. Applying the final value theorem to the transfer functions, Equations (40), assuming a unit step control input, confirms values for the static control gains,

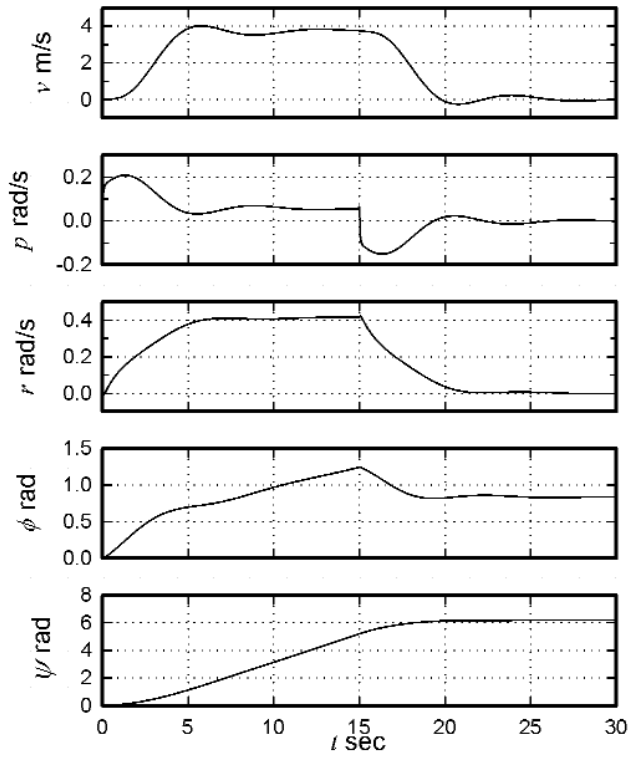

Figure 22. Lateral-directional response to 1 rad/15s square pulse input.

$$
\begin{aligned}
v_{ss} &= 3.77\xi \ \text{ m/s/rad} \\
p_{ss} &= 0.056\xi \ \text{ 1/s} \\
r_{ss} &= 0.428\xi \ \text{ 1/s}
\end{aligned}
\qquad \ldots (42)
$$

These values are consistent with the flight mechanics model of the hang glider although the values indicate that lateral-directional control sensitivity is much lower than for longitudinal control.

10.0 HANG GLIDER CONTROL

In view of the foregoing it is interesting to review the mechanics of hang glider control. The instantaneous longitudinal and lateral control derivatives referred to body axes, Equations (25), may be referred to wind axes for convenience (α_e = 0) and expressed in dimensionless coefficient form,

$$
\begin{aligned}
M^*_\delta &= \frac{m_p l_2}{mc'} \text{Cos}\,\delta_e \left(\begin{array}{l} C_{L_w} \text{Cos}\,\delta_e \\ + \left(C_{D_w} - \dfrac{m_w}{m_p} C_{D_p} \right) \text{Sin}\,\delta_e \end{array} \right) \\
L^*_\xi &= \frac{m_p l_2}{mb} C_{L_w} \text{Cos}\,\delta_e \\
N^*_\xi &= -\frac{m_p l_2}{mb} \left(C_{D_w} - \frac{m_w}{m_p} C_{D_p} \right) \text{Cos}\,\delta_e
\end{aligned}
\qquad \ldots (43)
$$

When Equations (43) are evaluated for a given flight condition, it is found that the instantaneous values of both the roll and yaw control derivatives are significant and, most importantly, N^*_ξ has a negative

sign. Solution of the equations of motion for this temporary condition shows significant adverse roll-yaw coupling in the initial response to a turn command. Clearly this is due to the adverse yawing moment created by the wing and pilot drag.

Once a commanded turn is established the adverse yawing control moment washes out to zero very quickly, as described earlier, and the non-zero control derivatives may be written,

$$M^*_\delta = \bar{M}_{p_{long}} \text{Cos}\ \delta_e \left(\begin{array}{l} C_{L_w} \text{Cos}\ \delta_e \\ + \left(C_{D_w} - \dfrac{m_w}{m_p} C_{D_p} \right) \text{Sin}\ \delta_e \end{array} \right) \qquad \ldots (44)$$

$$L^*_\xi = \bar{M}_{p_{lat}} C_{L_w} \text{Cos}\ \delta_e$$

where $\bar{M}_{plong}$ and $\bar{M}_{plat}$ are longitudinal and lateral pilot moment ratios respectively, as originally defined and described by Cook[6]. Pilot moment ratio has a meaning similar to that of the tail volume parameter in conventional aeroplanes. The pilot moment ratio may be interpreted as a control gain parameter and determines the control sensitivity. Thus control sensitivity may be increased by increasing the mass of the pilot, or by increasing the length of the hang strap, or both. Clearly, increased pilot mass has a performance penalty whereas hang strap length is governed only by hang glider geometry.

Equations (44) show that pitch and roll control of the hang glider is an aerodynamic phenomenon and has little to do with pilot weight shift. By moving himself relative to the wing, the pilot varies the *cg* position of the hang glider and by so doing generates control moments from the aerodynamic forces. The pilot does not generate control moments directly. Maximum available control moments are limited by geometry only, provided the wing is flying normally, which is dependent on the length of the pilot's arm.

11.0 CONCLUSIONS

11.1 Modelling

It is relatively straightforward to derive the equations of motion for the hang glider from those of the conventional aeroplane by including terms allowing for the variation in *cg* position caused by the suspended pilot mass. This leads naturally to the definition of equivalent aerodynamic stability derivatives which include the effects of *cg* variation. Although the resulting algebraic model is rather more complex, the formulation permits easy interpretation in the usual way. That this approach is appropriate is confirmed by the numerical solution of the equations of motion which leads to an entirely plausible description of the hang glider dynamics.

Aerodynamic modelling was based on limited aerodynamic data for a fifth generation hang glider wing – the Hiway Demon, which were obtained experimentally from full scale measurements using a purpose built mobile test rig. A mathematical model was developed to include twist and camber variation due to the extreme flexibility of the wing and this was matched to the experimental data empirically. The aerodynamic stability and control derivatives were derived from the mathematical aerodynamic model to produce values which seemed appropriate for the hang glider. It must be remembered that very little information is available in the literature with which to compare the derivative estimates.

11.2 Stability

Solution of the linearised equations of motion shows stability and response properties which are surprisingly consistent over the flight envelope in spite of the extreme flexibility of the wing. With the exception of the longitudinal phugoid mode, all modes show conventional characteristics but with a tendency toward higher than usual degrees of stability. Deviations from the norm were investigated through their governing derivatives and were found to be dependent on the peculiarities of the hang glider.

Since the wing structure stiffens up as speed increases the aerodynamic loading on the wing, the magnitudes of the stiffness derivatives vary accordingly. This has the effect of increasing the short term mode frequency, or shortening mode time constant as speed increases. This is most evident in the short period pitching mode, the Dutch roll mode and the roll subsidence mode.

A greater additional contribution to rotational stiffness of the hang glider is due to the suspended pilot mass which lowers the *cg* significantly. This creates a pendulum stability property which increases the degree of static stability in both pitch and roll. Most noticeably, this appears to dominate the roll subsidence mode dynamics and leads to a nominally constant value of the mode time constant.

The pendulum stability characteristic is also believed to contribute significantly to the high degree of stability exhibited by the spiral mode. The natural stabilising effect of the swept wing in this context is enhanced significantly and leads to a heavily damped mode with an unusually short stable time constant.

The phugoid mode stability shows the largest departure from the norm. Although usually very lightly damped its stability is around neutral in most conventional aeroplanes. However, for the hang glider the magnitude of the damping is higher than usual and it is unstable at the lowest speeds. Further, the frequency is significantly higher than usual and is sufficiently close to the short period pitching mode frequency that motion coupling might be expected. Whether or not this is the case is masked by the very high damping of the short period mode. A simple analysis readily reveals the cause of the unusual phugoid characteristics to be wing flexibility.

It is known that wing flexibility leads to significant variations in pitching moment with speed and that estimation of the property is least reliable at lower speeds. This gives rise to a significant non-zero estimate of the value of the pitching moment due to speed M_u derivative and, furthermore it is positive (de-stabilising) except at the very highest speed. For conventional aeroplanes this derivative is zero at low speeds. The value of the derivative is such that it has a significant influence on both phugoid damping and frequency to produce the result observed. However, confidence in the value of the derivative is low at the lowest speed and improves with increasing speed. As speed increases, the wing becomes more rigid in its shape due to aerodynamic loading and the value of the derivative diminishes in accordance with conventional understanding. It is therefore likely that the phugoid dynamics are more accurately modelled at the higher speeds, where the mode is stable.

11.3 Control

The hang glider control method is fundamentally aerodynamic. Weight shift control commands result in the wing lift and drag vectors being offset with respect to the hang glider *cg*, thereby generating control moments. This implies that control moments can, in principle, be generated irrespective of glider attitude and provided the wing is flying normally.

An instantaneous adverse yaw control input is an unavoidable consequence of a roll input due to the couple created by the drag vectors of the wing and pilot being offset from the hang glider cg in the *x*-*y* plane.

Longitudinal control sensitivity is approximately 1:1, such that the pitch attitude change is approximately equal to the control angle command. Lateral-directional control sensitivity is very much lower and is accompanied by a significant transient adverse response immediately following a lateral control input. The dynamic effectiveness of the controls is governed by the pilot moment ratio parameter $\bar{M}_p$ which is a control gain dependent on the mass of the pilot and hang strap length.

ACKNOWLEDGEMENTS

The authors are indebted to a number of former students who have undertaken thesis projects contributing to the understanding of the stability and control of the hang glider. In particular, the original PhD research contribution by Elizabeth Kilkenny led to the establishment of a validated aerodynamic model of the flexible hang glider wing on which all subsequent work has been based. Of direct relevance to the present research was the aerodynamic modelling of the flexible wing undertaken by John Powton as an MSc thesis project. This work enabled the subsequent development of dynamic models leading to the flight dynamics analysis described in this paper.

REFERENCES

1. KILKENNY, E.A. An Experimental Study of the Longitudinal Aerodynamic and Static Stability Characteristics of Hang Gliders, 1986, PhD thesis, College of Aeronautics, Cranfield Institute of Technology.
2. KILKENNY, E.A. An evaluation of a mobile aerodynamic test facility for hang glider wings, November 1983, College of Aeronautics Report 8330, Cranfield Institute of Technology.
3. COOK, M.V. and KILKENNY, E.A. An experimental investigation of the aerodynamics of the hang glider, 1986, Paper No 25, Proceedings of an International Conference on Aerodynamics at low Reynolds numbers, October 1986, Royal Aeronautical Society, London.
4. KILKENNY, E.A. Full scale wind tunnel tests on hang glider pilots, 1984, College of Aeronautics Report 8416, Cranfield Institute of Technology.
5. BLAKE, D.M. Modelling the aerodynamics, stability and control of the hang glider, 1991, MSc thesis, College of Aeronautics, Cranfield Institute of Technology.
6. COOK, M.V. The theory of the longitudinal static stability of the hang-glider, *Aeronaut J*, October 1994, **98**, (978), pp 292-304.
7. POWTON, J.N. A Theoretical Study of the Non-linear Aerodynamic Pitching Moment Characteristics of the Hang Glider and its Influence on Stability and Control, 1995, MSc thesis, College of Aeronautics, Cranfield University.
8. ROLLINS, R. Study of Experimental Data to Assess the Longitudinal Stability and Control of the Hang Glider, 2000, MSc thesis, College of Aeronautics, Cranfield University.
9. SPOTTISWOODE, M. A Theoretical Study of the Lateral-directional Dynamics, Stability and Control of the Hang Glider, 2001, MSc thesis, College of Aeronautics, Cranfield University.
10. KROO, I. Aerodynamics, Aeroelasticity and Stability of Hang Gliders, 1983, PhD thesis, Stanford University.
11. DE MATTEIS, G. Response of hang gliders to control, *Aeronaut J*, October 1990, **94**, (938), pp 289-294.
12. DE MATTEIS, G. Dynamics of hang gliders, *AIAA J Guidance, Control and Dynamics*, November-December 1991, **14**, (6).
13. COOK, M.V. *Flight Dynamics Principles*, 1997, Arnold, London.
14. SWEETING, J.T. An Experimental Investigation of Hang Glider Stability, 1981, MSc thesis, College of Aeronautics, Cranfield University.
15. NICKEL, K and WOHLFAHRT, M. *Tailless Aircraft*, 1990, Ch 9, pp 385-420, Edward Arnold, London.
16. ESDU: Validated engineering data – Aerodynamics series, Engineering Sciences Data, Data Items 79006 and 90010, ESDU International, London.